國立臺灣大學醫療器材與醫學影像研究所

碩士論文

Graduate Institute of Medical Device and Imaging
College of Medicine
National Taiwan University

Master's Thesis

電腦輔助皮質骨軌跡螺釘植入：以粒子群最佳化演算法提升螺釘植入準確度

Computer-Assisted Cortical Bone Trajectory Screw Placement: Precision Enhancement through Particle Swarm Optimization (PSO)

周宜菜

Yi-Rou Chou

指導教授：蕭輔仁 博士

Advisor: Furen Xiao, Ph.D.

中華民國 115 年 8 月

August, 2026

doi:10.6342/NTU202604598

誌謝

來到醫材影像所的日子轉瞬即逝，猶記得入學前拜訪蕭醫師的畫面，那時老師也剛進入醫材影像所不久，我便成了老師簽下的第一位正式學生。一直很感謝老師對我的寬容，雖說老師本身給每位學生的自由度皆很高，但能忍受學生自己主動想找其他硬體實驗室共指、四處拜訪別的研究室，到生醫電資所一學期又回來的教授應該真的找不到第二位，能被這樣包容與接受，實屬我的福氣與幸運。另外，也總體諒著我家境不甚理想的處境，找機會讓我當助教、幫忙研究計畫，讓北上生活的我獲得了很多幫助，對老師真的是滿滿的感恩。

在升上碩二時回到了醫材影像所，剛好銜接上陳敏弘醫師的研究計畫，能認識到陳醫師、成為陳醫師共同指導的學生也讓我感到非常榮幸，陳醫師總是會在每次聽我報告後給予很多臨床上的見解，提供我相當不同的視野與研究方向，也讓我的研究能在兼顧臨床的狀況下前進，而非僅是一個滿足數學運算的演算法。此外，也非常感謝廖俊智醫師擔任我的口試委員，廖醫師總是相當認真、仔細地提供我許多意見與各方面的提點，讓我的論文在一次次的修正下愈來愈完整，是我能完成這篇論文的一大功臣。

再來，也相當感謝實驗室一起的夥伴，感謝 Zola 總是替我的程式問題解惑，以及擔任我的英文口說練習對象，在碩士班的時間裡我的英文能夠有所進步，很大一部分是 Zola 的功勞。另外，和已經畢業的薇瑛、育暄還有羽軒一起當蕭醫師的第一屆學生是相當有趣的回憶。

感謝我的家人總是非常支持我，儘管不知道我申請什麼研究所、到底在做什麼研究也依然以我為榮。感謝身邊的小高，一路陪我從臺南到臺北打拼，讓我在臺北的生活不曾孤立無援。

最後，感謝 NVIDIA 的運算資源，也感謝一路上遇見的人，這些相遇皆成為了我的養分，碩士班的時光讓我逐漸茁壯、成為了不一樣的自己，謝謝大家。

doi:10.6342/NTU202604598

中文摘要

椎弓根螺釘（Pedicle Screws, PS）固定手術是脊椎手術中的主要技術。然而，對於骨質密度較低或骨質疏鬆的患者，傳統螺釘植入方式面臨了固定效果不足和鬆脫的風險。本研究關注近年發展的皮質骨軌道（Cortical Bone Trajectory, CBT）螺釘植入技術，此技術由 Santoni 研究團隊於 2009 年提出。CBT 技術透過將螺釘路徑調整為矢狀面上的尾向頭及橫切面上的由內向外方向，能夠有效增加螺釘與皮質骨的接觸面積，進而強化螺釘的固定力和界面強度。相較於傳統螺釘植入方式，CBT 螺釘具備更優異的固定能力、恢復期較短、減低術後併發症等優勢。

然而，儘管 CBT 優勢顯著，但其植入路徑之準確性是決定手術成敗的關鍵。由於 CBT 螺釘植入角度與傳統技術的手感差異大，難以單純透過術者的經驗精準掌握，若植入不當，可能危及脊髓、神經根及椎動脈等周圍重要結構。因此，術前精確規劃螺釘植入路徑成為確保手術安全性和固定效果的重要前提。

為了提升 CBT 螺釘植入的準確性、安全性和固定效果，本研究旨在開發一套電腦輔助的自動化術前規劃系統。我們利用醫學影像技術結合人工智慧，以粒子群最佳化（Particle Swarm Optimization, PSO）演算法作為核心工具，根據每位患者的 CT 影像、其獨特的脊椎解剖結構和臨床需求，量身制定皮質骨軌道螺植入之最佳位置。此系統的開發旨在協助臨床醫師進行更精準的術前決策，從而提升手術成功率並且降低併發症發生的風險。

關鍵字：椎弓根螺釘、皮質骨軌道、脊椎手術、自動化術前規劃、粒子群最佳化

doi:10.6342/NTU202604598

ABSTRACT

Pedicle Screw (PS) fixation is a widely applied technique in spinal surgery. However, in patients with low bone mineral density or osteoporosis, conventional screw placement often faces challenges related to poor fixation strength and the risk of loosening. This study focuses on the more recently developed implant technique: Cortical Bone Trajectory (CBT), first proposed by Santoni's research team in 2009.

The CBT technique modifies the screw trajectory to follow a caudal-to-cephalad path in the sagittal plane and a medial-to-lateral path in the axial plane. This innovation significantly increases the contact area between the screw thread and the dense cortical bone, thereby enhancing screw pullout strength and interface rigidity. Compared to traditional spinal fusion and fixation surgeries, CBT screws offer superior fixation capacity, minimal invasiveness, and a shorter recovery period.

Despite its advantages, the success of CBT is critically dependent on the accuracy of the screw insertion trajectory. Since the tactile feedback (hand-feel) of CBT placement differs substantially from that of traditional PS placement, accurate spatial orientation becomes challenging. Incorrect placement poses severe risks to surrounding vital structures, including the spinal cord, nerve roots, and vertebral arteries. Therefore, precise pre-operative planning is an essential step to ensure optimal fixation and minimize the risk of complications.

To improve the efficacy, accuracy, and safety of CBT screw placement, this research aims to develop a computer-aided, automated pre-operative planning system. We integrate CT images (Computed Tomography images) with artificial intelligence, utilizing the Particle Swarm Optimization (PSO) algorithm as the core computational tool. This system is designed to individually tailor the optimal position and trajectory for CBT

doi:10.6342/NTU202604598

pedicle screw placement based on each patient's unique anatomical structure and specific needs. The goal is to assist surgeons in precise pre-operative decision-making, enhance screw placement accuracy, and ultimately reduce the incidence of complications.

Keywords—Pedicle screw placement, cortical bone trajectory (CBT), spinal surgery, automatic surgical planning, particle swarm optimization (PSO)

doi:10.6342/NTU202604598

CONTENTS

誌謝 i

中文摘要 ii

ABSTRACT iii

CONTENTS v

LIST OF FIGURES viii

LIST OF TABLES x

Chapter 1 Introduction 1

1.1 Research Background 1

1.1.1 Spine Diseases 2

1.1.2 Spine Fixation and Fusion Surgery 5

1.1.3 Pedicle Screws 6

1.1.4 Cortical Bone Trajectory (CBT) 7

1.2 Research Motivation 10

1.3 Literature Review 14

1.4 Research Objectives 15

1.5 Novelty of the Study 19

Chapter 2 Theoretical Background 23

2.1 Fundamentals of Medical Image Analysis 23

2.1.1 CT Image Processing 23

2.1.2 Segmentation 26

2.2 Principles of Image-Based Surgical Planning 27

2.3 Particle Swarm Optimization (PSO) 29

doi:10.6342/NTU202604598

2.4 Comparative Optimization Algorithms....31
2.5 PyTorch Framework....32
2.6 Bresenham's Line Algorithm....34
Chapter 3 Methodology....36
3.1 CTSpine1K Dataset....36
3.2 Proposed Algorithm....41
3.3 A Projection-Based Approach for Calculating Vertebral Orientation....44
3.3.1 Azimuth....46
3.3.2 Altitude....48
3.4 Vertebral ROI Extraction and HU-based Bone Characterizationration (Thresholding methods)....50
3.4.1 Bone Mask Generation....50
3.4.2 Cortical-Oriented Mask Generation....52
3.4.3 HU-based Bone Density Interpretation....54
3.5 Cylindrical Screw Representation....56
3.6 Objective Fuction Design....58
3.7 Implementation Details....59
Chapter 4 Results....61
4.1 Sensitivity Analysis of PSO Hyperparameters....61
4.1.1 Experimental Setup....62
4.1.2 Effect of Swarm Size and Iteration Count....62
4.2 Performance Evaluation of the Proposed Method....66
4.2.1 Iterative Optimization Process of the PSO Algorithm....66
4.2.2 Lumbar Spine Results (L1-L5)....67
4.3 Comparison with State-of-the-Art....71

doi:10.6342/NTU202604598

Chapter 5 Discussion.....73

5.1 Angular Deviation 73

5.2 Anatomical Constraints 73

5.3 Thread Modeling Limitation.....75

Chapter 6 Conclusion and Future Work.....77

6.1 Conclusion 77

6.2 Future Work 78

REFERENCE 80

APPENDIX 85

doi:10.6342/NTU202604598

LIST OF FIGURES

Fig. 1 Surgical technique of cortical bone trajectory (A–D) and traditional pedicle screws (E–H) (adapted from [6]).....2

Fig. 2 Spine and intervertebral disc anatomy (adapted from [8]).....3

Fig. 3 Comparison of cortical bone trajectory and pedicle trajectory (adapted from [25]).....8

Fig. 4 Python implementation for loading NIFTI (.nii.gz) using the nibabel library. 24

Fig. 5 2D particle swarm optimization visualization.....30

Fig. 6 3D particle swarm optimization visualization.....30

Fig. 7 2D bresenham line.....35

Fig. 8 Examples of CTSpine1K dataset (adapted from [38]). 36

Fig. 9 Illustration of the seven parameters optimized in the PSO framework.....42

Fig. 10 Examples of segmented L5 vertebrae from five patients. 44

Fig. 11 Estimation of vertebral axial orientation using the top-point–centroid axis 47

Fig. 12 Estimation of vertebral sagittal orientation for altitude angle determination.....49

Fig. 13 **Visualization of the preprocessing and mask generation pipeline for the L5 vertebra.** (a) Original ROI: The initial cropped region containing the patient's L5 vertebra, including the surrounding anatomical background. (b) Segmented ROI: The isolated L5 region obtained after background removal using label-based segmentation, focusing strictly on the vertebral structure. (c) Binary Bone Mask: A complete binary representation of the ROI where all internal pixels are assigned a value of 1. 53

Fig. 14 HU Distribution within the vertebral region-of-interest (ROI) of a representative

doi:10.6342/NTU202604598

subject 56
Fig. 15 Heatmaps of the PSO hyperparameter sensitivity analysis. 65
Fig. 16 Snapshots of the screw trajectory optimization process. 66
Fig. 17 Representative cortical bone trajectory (CBT) planning results for lumbar vertebrae (L1–L5) 70
Fig. 18 Representative example of distal tip breach in upper lumbar cortical bone trajectory (CBT) 74

doi:10.6342/NTU202604598

LIST OF TABLES

Table 1 Statistical distribution of annotated vertebral levels in the COLONOG subset (N=784). 40

Table 2 Representative cortical bone trajectory (CBT) planning results for lumbar vertebrae (L1–L5). 69

Table A 1. Performance metrics for anatomical segmentation across tested configurations (Swarm Size vs. Iterations): Cortical and Vertebral bone analysis. 86

Table A 2. Cortical-to-trabecular ratio and computational runtime metrics across tested configurations (Swarm Size vs. Iterations). 87

doi:10.6342/NTU202604598

Chapter 1 Introduction

1.1 Research Background

Due to the aging population and the increasing prevalence of osteoporosis, spinal diseases have become a common health problem. Over the past few decades, the global burden of low back pain has steadily increased. According to the Global Burden of Disease Study [3],approximately 619 million individuals were affected by low back pain in 2020, and this number is projected to rise to reach 843 million by 2050. Besides, neck pain affected an estimated 203 million individuals worldwide in 2020, with projections indicating an increase to 269 million by 2050. All of these issues are strongly associated with spinal conditions.

Spinal fusion surgery, for instance, is a procedure that connects two or more vertebrae in the spine, and is commonly used to treat conditions such as spinal fractures, spondylolisthesis, and spondylosis. The traditional trajectory (TT) technique for transpedicular screw (TPS) fixation ,which is regarded as the main surgical method for spinal fixation and fusion, is widely applied and generally effective in most cases. However, in patients with osteoporosis or specific anatomical variations, it may result in insufficient fixation strength, increasing the risk of screw loosening or failure.

In 2009, Santoni et al. proposed an alternative technique known as cortical bone trajectory (CBT)[5]. CBT is an advanced method for pedicle screw placement that modifies the traditional trajectory to follow a medial-to-lateral and caudal-to-cephalad path, engaging the denser cortical bone. This technique increases the contact area between the screw and the denser cortical bone [6], leading to improved biomechanical stability, enhanced fixation strength, and reduced surgical invasiveness.

doi:10.6342/NTU202604598

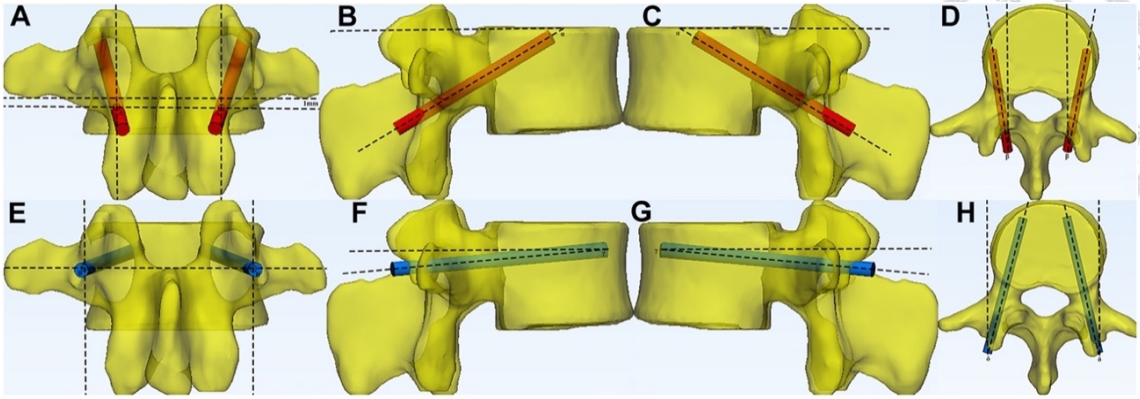

Fig. 1 Surgical technique of cortical bone trajectory (A–D) and traditional pedicle screws (E–H) (adapted from [6]).

1.1.1 Spine Diseases

With the aging of the global population, the incidence of spinal disorders is steadily increasing. Age-related degeneration of the spine is among the leading causes of disability or other discomforts in daily life for elderly people. Degenerative conditions such as lumbar spondylosis, spinal stenosis, and osteoporosis-related vertebral fractures lead to more serious problems and are becoming more prevalent among the elderly. People with spine diseases might suffer from a series of related problems such as chronic pain, neurological deficits, and stiffness, leading to a reduced quality of life.

For instance, degenerative disc disease (DDD) is a prevalent condition and a primary contributor to spine problems among older adults, with studies indicating it affects individuals above the age of 45 [7]. Although DDD is a disease, it is fundamentally a consequence of the natural aging process. Intervertebral discs, which are positioned between vertebrae, serve as crucial shock absorbers between adjacent vertebral bodies, mitigating compressive forces experienced by the spine. As intervertebral discs age, they gradually lose their elasticity and diminish in water content. This loss of functional capacity results in discomfort and limitation of spinal mobility. The primary symptoms

doi:10.6342/NTU202604598

of lumbar disc degeneration include lower back pain and sciatica, which are often exacerbated by activities such as standing, walking, bending, straining, or coughing. This combination of chronic discomfort and restricted mobility necessitates effective therapeutic interventions aimed at restoring the patient's quality of life.

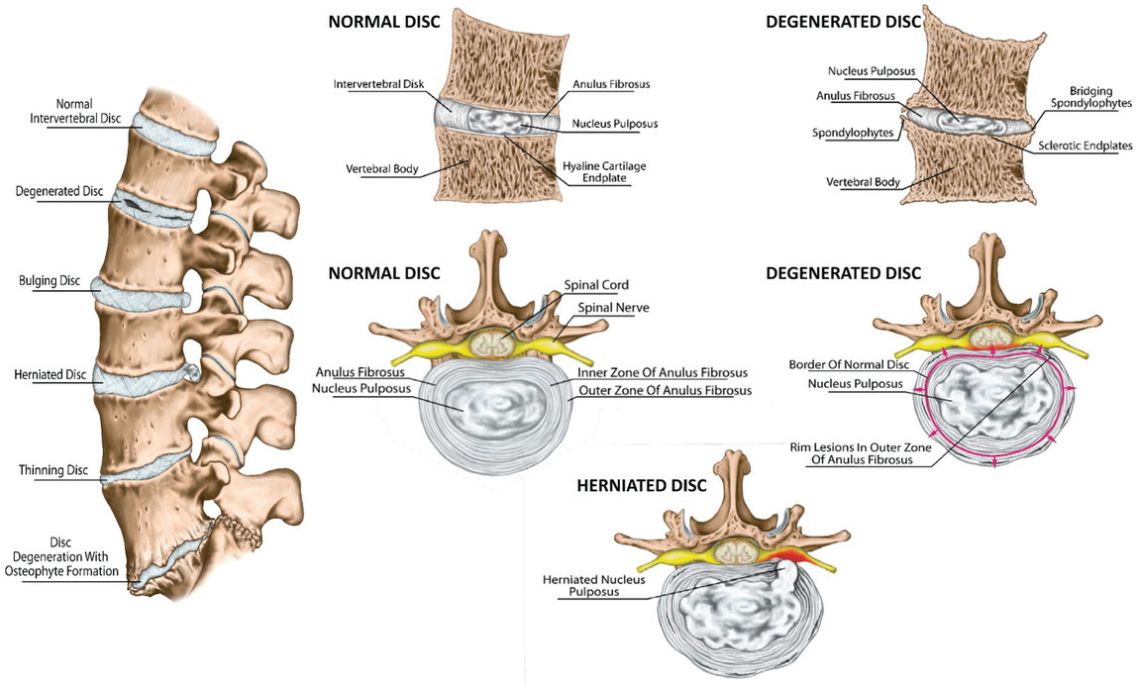

Fig. 2 Spine and intervertebral disc anatomy (adapted from [8]).

Beyond degenerative disc disease, several other spinal pathologies significantly contribute to the burden of spine-related disabilities. Lumbar spinal stenosis, characterized by the narrowing of the spinal canal, commonly results from age-related changes including facet joint hypertrophy, ligamentum flavum thickening, and disc bulging [9]. This progressive narrowing compresses neural structures, leading to neurogenic claudication—a condition manifesting as leg pain, numbness, and weakness that worsens with ambulation and improves with rest or forward flexion [10]. Spondylolisthesis, another prevalent condition particularly among the elderly, involves the forward or backward displacement of one vertebra relative to an adjacent vertebra [11]. This misalignment can occur due to degenerative changes in the facet joints and

doi:10.6342/NTU202604598

intervertebral discs, potentially causing spinal instability, nerve compression, and chronic lower back pain that radiates to the lower extremities [12].

Additionally, spinal deformities such as degenerative scoliosis represent a growing concern in the aging population. Unlike adolescent idiopathic scoliosis, adult degenerative scoliosis develops as a result of asymmetric disc degeneration and facet joint arthritis, leading to progressive spinal curvature that can cause pain, postural imbalance, and neurological compromise [13]. These conditions often coexist with other degenerative pathologies, compounding the complexity of clinical management [14].

On the other hand, osteoporosis-related complications present distinct yet equally significant challenges in spinal care. Osteoporosis, a systemic skeletal disorder characterized by reduced bone mineral density and deterioration of bone microarchitecture, renders vertebrae increasingly susceptible to fractures even under minimal trauma [15]. Vertebral compression fractures (VCFs), the most common osteoporotic fractures, can occur spontaneously or following minor activities such as bending or lifting [16]. These fractures severely impact a patient's quality of life, causing acute or chronic pain, progressive spinal deformity (kyphosis), reduced pulmonary function, and increased risk of subsequent fractures [17]. The presence of osteoporotic bone also poses substantial challenges during surgical intervention, as compromised bone quality affects the fixation strength of implants, potentially leading to screw loosening, construct failure, and pseudarthrosis [18], [19].

As a result, the demand for spinal surgical interventions, including spinal fixation and fusion procedures, has significantly increased, emphasizing the need for precise and effective surgical planning to improve patient outcomes in this growing patient population [20]. Achieving optimal surgical outcomes in these complex cases necessitates advanced planning tools that can accommodate individual anatomical variations and ensure

doi:10.6342/NTU202604598

maximum fixation strength.

1.1.2 Spine Fixation and Fusion Surgery

Spinal fusion is a widely performed surgical procedure designed to join two or more vertebrae, thereby eliminating motion at an unstable spinal segment and providing long-term stability. This technique is primarily indicated for correcting spinal deformities, stabilizing fractures, and alleviating pain associated with conditions such as degenerative disc disease, scoliosis, spondylolisthesis, and spinal stenosis [1], [4]. The procedure typically involves placing a bone graft or bone substitute material between the affected vertebrae, which gradually integrates and fuses them into a single, solid structure during the healing process.

To facilitate successful fusion, spinal fixation using metallic implants—including screws, rods, and plates—is routinely employed to provide rigid stabilization during the critical bone healing period. These fixation devices serve multiple essential functions: they maintain proper spinal alignment, resist physiological loads imposed by body weight and movement, and prevent micromotion at the fusion site that could compromise bone integration. Among various fixation methods, pedicle screw-rod constructs have become the gold standard due to their superior biomechanical properties and versatility across different spinal pathologies.

The success of spinal fusion surgery is fundamentally dependent on achieving adequate mechanical stability through precise implant placement. The accuracy of pedicle screw positioning directly influences both the structural integrity of the construct and the safety profile of the procedure. Optimal screw trajectory, angulation, and sizing are critical factors that determine fixation strength, minimize the risk of neurovascular complications, and ultimately contribute to favorable long-term clinical outcomes. Consequently, advances in surgical planning and screw placement techniques remain a

doi:10.6342/NTU202604598

focal point in contemporary spinal surgery research.

1.1.3 Pedicle Screws

Pedicle screws represent the cornerstone of modern spinal fixation, serving as the primary anchoring mechanism in posterior spinal instrumentation. These specialized implants are inserted through the pedicles—the narrow bony bridges connecting the vertebral body to the posterior elements—providing robust three-column fixation that engages the anterior, middle, and posterior structural supports of the spine [18]. This biomechanical advantage enables pedicle screws to deliver superior pullout resistance and rotational stability compared to alternative fixation methods such as hooks, wires, or sublaminar bands.

First introduced by Boucher in the 1950s and subsequently refined over decade, pedicle screw fixation has become the standard of care for treating a broad spectrum of spinal disorders, including traumatic fractures, degenerative conditions, spinal deformities (e.g., scoliosis and kyphosis), spondylolisthesis, and tumors [21]. The versatility of pedicle screw systems allows surgeons to achieve powerful corrective forces, maintain anatomical alignment during fusion, and provide immediate postoperative stability that facilitates early patient mobilization.

However, the efficacy and safety of pedicle screw fixation are highly dependent on precise placement accuracy. The pedicle represents a relatively narrow anatomical corridor, bordered medially by the spinal canal containing neural structures, laterally by the nerve root, and anteriorly by major vascular structures. Consequently, even minor deviations from the optimal trajectory can result in serious complications, including nerve root injury, dural tears, cerebrospinal fluid leakage, vascular damage, or screw loosening due to cortical breach. The study reported that the overall median accuracy of pedicle screw placement without navigation was 90.3%, whereas the accuracy in the *in vivo*

doi:10.6342/NTU202604598

navigation-assisted subgroup reached 95.2% [22]. Despite the significant enhancement provided by navigation, the in vivo accuracy rate of 95.2% indicates that a finite risk of inaccurate placement (4.8%) remains.

Traditional pedicle screws are manufactured in various dimensions to accommodate anatomical variability across different vertebral levels, patient populations, and surgical indications. In adult lumbar spine surgery, pedicle screw diameters typically range from 4.5 mm to 7.5 mm, with 5.5 mm and 6.5 mm being the most frequently utilized sizes that balance adequate fixation strength with safety margins for cortical wall thickness. Screw lengths generally vary from 30 mm to 50 mm, with longer screws often employed in the lumbar region to maximize purchase within the vertebral body and enhance pullout resistance [23]. The selection of appropriate screw dimensions is a critical preoperative decision that requires careful analysis of computed tomography (CT) imaging to assess pedicle morphology, cortical thickness, and the spatial relationship to adjacent neurovascular structures. Optimal screw sizing must achieve sufficient anchorage for biomechanical stability while maintaining an adequate safety margin to prevent cortical breaches and associated complications.

1.1.4 Cortical Bone Trajectory (CBT)

To address some of the limitations associated with traditional pedicle screw fixation—particularly in osteoporotic bone, revision surgery scenarios, and minimally invasive approaches—Santoni and colleagues introduced an alternative technique known as cortical bone trajectory (CBT) screw fixation in 2009 [5]. Unlike conventional pedicle screws that follow the anatomical axis of the pedicle in a lateral-to-medial and slightly caudal trajectory, CBT screws utilize a medial-to-lateral path in the transverse plane combined with a caudal-to-cephalad trajectory in the sagittal plane (typically 25°–30°

doi:10.6342/NTU202604598

cranially) [24], [27].

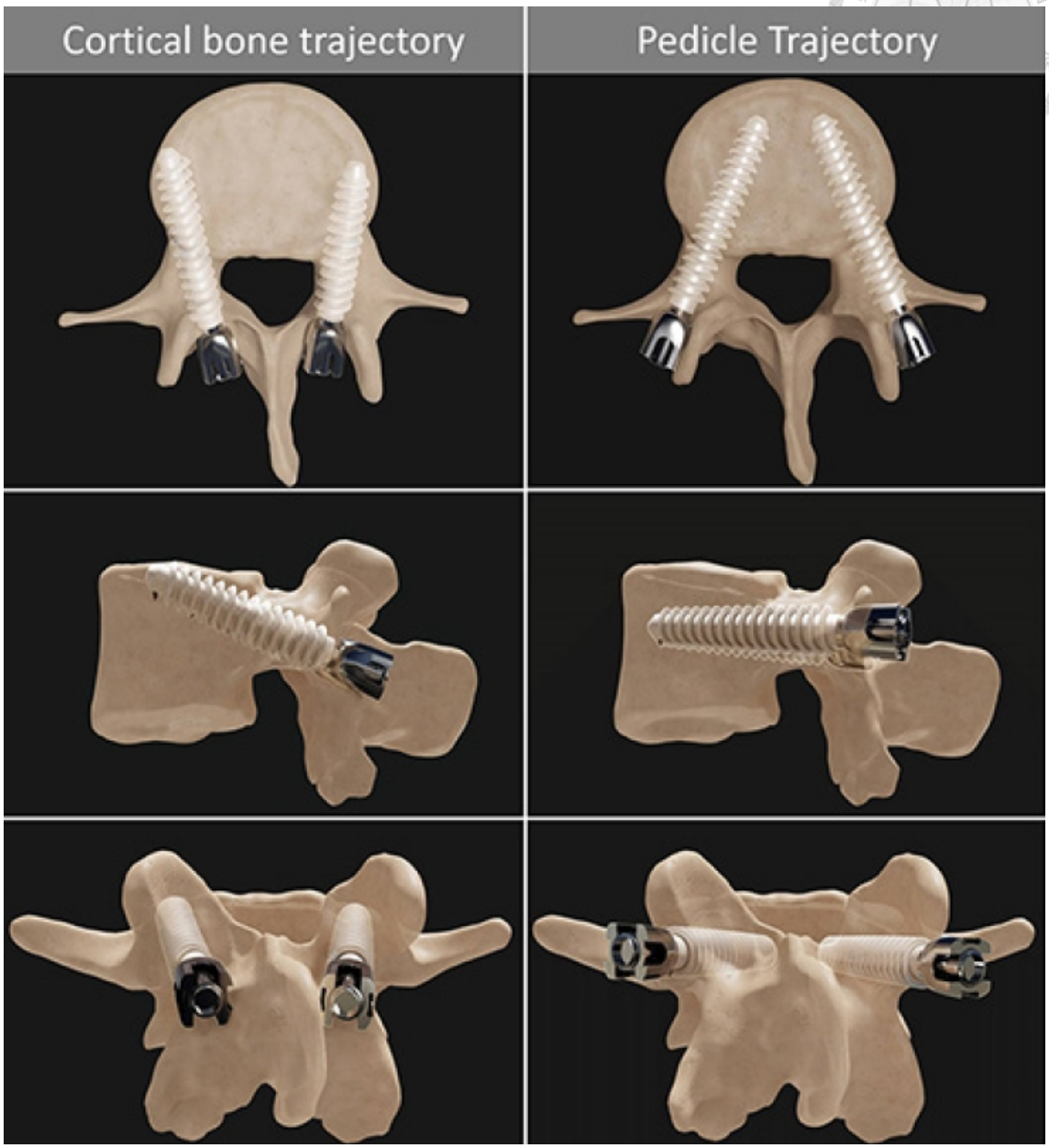

Fig. 3 Comparison of cortical bone trajectory and pedicle trajectory (adapted from [25]).

This unique trajectory is specifically designed to maximize contact with the higher-density cortical bone along the pedicle walls and lamina, rather than relying primarily on the softer cancellous bone within the vertebral body. The biomechanical rationale underlying CBT is that cortical bone is less susceptible to osteoporotic changes compared to trabecular bone, potentially offering superior screw purchase and resistance to

doi:10.6342/NTU202604598

loosening in patients with compromised bone quality [24], [26]. Additional proposed advantages of CBT include: (1) a more medial starting point that requires less extensive paraspinal muscle dissection, reducing surgical morbidity; (2) a reduced risk of superior facet joint violation, potentially lowering the incidence of adjacent segment degeneration; and (3) a trajectory that minimizes the risk of pedicle medial wall perforation and subsequent neural injury.

Due to the distinct trajectory and reliance on cortical bone engagement, CBT screws typically have different dimensional specifications compared to traditional pedicle screws. CBT screw diameters commonly range from 4.5 mm to 5.5 mm, and lengths typically span from 25 mm to 45 mm. Notably, the enhanced cortical bone purchase afforded by the CBT trajectory often allows for the use of shorter screws while maintaining comparable or even superior fixation strength relative to longer traditional pedicle screws.

In a biomechanical study by Santoni et al. [5], the mean overall length and diameter of CBT screws used in experimental testing were reported to be 29.00 ± 2.89 mm and 4.66 ± 0.24 mm, respectively, which were significantly smaller than those of traditional trajectory screws ($p < 0.001$). These findings further support the notion that CBT fixation can achieve sufficient mechanical stability with reduced implant dimensions, owing to improved cortical bone engagement.

Studies utilizing finite element analysis and cadaveric biomechanical testing have also suggested that CBT screws with a diameter of at least 5.5 mm and a length exceeding 35 mm provide optimal fixation strength in the lumbar spine [31]. Nevertheless, appropriate screw sizing in CBT remains highly dependent on individual patient anatomy, bone quality, and the specific surgical indication, necessitating careful preoperative planning based on three-dimensional imaging analysis.

Despite the theoretical and biomechanical advantages of CBT, clinical evidence

doi:10.6342/NTU202604598

comparing CBT to traditional pedicle screw fixation has yielded mixed results. While some studies have demonstrated comparable fusion rates, reduced surgical morbidity, and lower rates of screw-related complications with CBT [30], [31], other investigations have raised concerns about potential limitations in certain clinical scenarios, such as high-grade spondylolisthesis or severe spinal deformity correction, where the shorter lever arm and reduced rotational control of CBT screws may be disadvantageous [30]. Furthermore, the relatively recent introduction of CBT means that long-term outcome data remain limited compared to the extensive evidence base supporting traditional pedicle screw techniques.

The selection between traditional pedicle screw and CBT fixation, as well as the determination of optimal screw dimensions and trajectories, underscores the critical importance of precise preoperative surgical planning. Advanced computational tools capable of analyzing patient-specific anatomy, simulating screw trajectories, and optimizing screw parameters could significantly enhance surgical safety, improve fixation quality, and contribute to better clinical outcomes in an increasingly diverse patient population with varying anatomical characteristics and bone quality profiles.

1.2 Research Motivation

In general, compared to traditional transpedicular screw placement, the implantation of CBT is more technically challenging. The traditional trajectory (TT) technique for traditional TPS has well-defined anatomical landmarks for screw insertion, in contrast, the entry point for CBT is not easily identified by the naked eye, and the path involves denser cortical bone, which requires hammer insertion. Thus, CBT requires careful consideration of the screw insertion angle and bone quality. Existing literature has shown that preoperative CT evaluation can improve screw accuracy and reduce complications

doi:10.6342/NTU202604598

[33]. Furthermore, placing the screw in a position with more cortical bone engagement significantly enhances the outcome. However, even with preoperative CT scans, less experienced surgeons may struggle to determine the optimal entry point and angle.

Despite the potential biomechanical and clinical advantages of cortical bone trajectory (CBT) screw fixation, its implementation presents considerable technical challenges that have limited its widespread adoption in clinical practice. Compared to traditional transpedicular screw (TPS) placement, which benefits from well-established and readily identifiable anatomical landmarks—such as the intersection of the lateral border of the superior articular facet and the midline of the transverse process—CBT screw insertion requires substantially greater surgical precision and anatomical understanding.

The technical difficulties inherent to CBT stem from several factors. First, the entry point for CBT screws, located at the junction of the center of the superior articular process and approximately 1 mm inferior to the inferior border of the transverse process [28], is not easily visualized or palpated intraoperatively, particularly in minimally invasive surgical approaches. Second, the medial-to-lateral and caudal-to-cephalad trajectory must be executed with strict adherence to the recommended angulation (typically 25°–30° cranially and 10° laterally) to maximize cortical bone engagement while avoiding breaches of the pedicle cortex or lamina [27]. Third, unlike traditional TPS insertion through predominantly cancellous bone, the CBT path traverses denser cortical bone structures, often necessitating bone tapping or even controlled hammering for screw advancement, which increases the risk of inadvertent pars interarticularis fracture, particularly in osteoporotic or spondylolytic vertebrae [32].

The complexity of CBT placement is further compounded by substantial inter-individual anatomical variability in pedicle morphology, cortical thickness, and vertebral

doi:10.6342/NTU202604598

dimensions across different spinal levels and patient populations. This anatomical heterogeneity means that a standardized "one-size-fits-all" approach to CBT screw sizing and trajectory determination is inadequate. Consequently, meticulous preoperative planning based on detailed three-dimensional imaging analysis has become increasingly recognized as essential for successful CBT implementation [33].

Existing literature has demonstrated that comprehensive preoperative computed tomography (CT) evaluation can significantly improve screw placement accuracy, reduce complication rates, and optimize fixation strength. Advanced imaging analysis enables surgeons to assess critical anatomical parameters, including pedicle width and height, cortical bone thickness, optimal screw trajectory angles, and maximum permissible screw dimensions for each individual vertebra. Furthermore, research has established that maximizing cortical bone contact along the screw thread trajectory is a key determinant of fixation strength, particularly in osteoporotic bone where trabecular support is compromised [23]. Therefore, the ability to identify screw trajectories that optimize cortical bone engagement while maintaining adequate safety margins from neurovascular structures represents a critical objective in CBT surgical planning.

However, despite the availability of high-resolution preoperative CT imaging, the manual interpretation and trajectory planning process remains highly dependent on surgeon experience and expertise. Less experienced surgeons often encounter difficulties in accurately determining the optimal entry point, insertion angle, and screw dimensions from two-dimensional CT slices or even three-dimensional reconstructions [34]. The cognitive challenge of mentally translating complex three-dimensional anatomical information into precise intraoperative surgical execution can lead to suboptimal screw placement, increased operative time, and elevated complication risk. Even among experienced surgeons, inter-operator variability in trajectory planning and execution

doi:10.6342/NTU202604598

remains a recognized limitation [35].

Moreover, current clinical practice typically relies on qualitative visual assessment of CT scans rather than quantitative, systematic optimization of screw parameters. Surgeons generally select screw sizes from available implant inventories based on subjective estimation of anatomical fit, rather than through rigorous computational analysis of the trajectory that would maximize cortical bone engagement while ensuring safe clearance from critical structures. This limitation is particularly relevant for CBT, where the unique trajectory and reliance on cortical bone contact make trajectory optimization more complex than in TT placement.

These challenges highlight a critical unmet need in contemporary spinal surgery: the development of objective, quantitative, and automated computational tools that can analyze patient-specific CT imaging data and systematically determine the optimal CBT screw trajectory and dimensions for each individual vertebra. Such tools would not only assist less experienced surgeons in achieving placement accuracy comparable to experts but would also provide experienced surgeons with decision support that could further enhance surgical precision and outcomes. Furthermore, an automated optimization approach could potentially identify superior trajectories that maximize cortical bone engagement beyond what might be achieved through manual planning alone.

Therefore, this study aims to develop and validate a novel automated computational framework for optimizing cortical bone trajectory screw placement using particle swarm optimization (PSO) algorithms applied to patient-specific CT imaging data. The proposed method seeks to objectively identify the optimal screw entry point, trajectory angles, diameter, and length that maximize cortical bone contact while maintaining safe distances from anatomical boundaries, thereby addressing the current limitations of manual surgical planning and improving safety and efficacy of CBT screw fixation procedures.

doi:10.6342/NTU202604598

1.3 Literature Review

Matsukawa et al. [23], [27] - [30] suggested that the ideal cortical bone trajectory (CBT) for lumbar pedicle screw insertion should project in the 5 o'clock orientation for the left pedicle and the 7 o'clock orientation for the right pedicle. In their 2015 study, they found the optimal trajectory length to be between 36–39 mm, with a lateral angle of 8–9 degrees and a cephalad angle of 25–26 degrees. They further emphasized that factors such as the cephalad angle, screw length within the lamina, and the patient's bone mineral density (BMD) significantly influenced screw fixation strength, recommending a cranial angulation of 25°-30° for the ideal sagittal trajectory.

In a subsequent 2020 study, Matsukawa et al. demonstrated that the screw diameter had a substantial impact on pullout strength, with this effect not being limited to screws with a diameter of 6.5 mm. F. Penner et al. [33] proposed that screws should have a minimum length of 35–40 mm and a minimum diameter of 5.5 mm to maximize bone purchase and ensure optimal fixation strength. Additionally, Z. Yong-Hui et al. [36] provided further details on the cephalad and lateral angles, with the cephalad angle ranging from 26.49 ± 3.84 mm to 41.94 ± 6.05 mm, and the lateral angle between 19.63 ± 4.54 mm and 22.16 ± 4.25 mm across L1-L5.

Meanwhile, Delgado-Fernández et al. [37] employed intraoperative 3D fluoroscopy and Brainlab-based navigation for spinal screw placement training. They used screws with diameters of 5.5 mm and lengths ranging from 35 to 45 mm, positioned at the 5 o'clock position for the left pedicle and 7 o'clock for the right pedicle, adopting a cranio-caudal angulation of 25°-30° toward the superior endplate to simulate the ideal cortical bone trajectory.

To enhance the effectiveness, accuracy, and safety of screw implantation, various

doi:10.6342/NTU202604598

assistive technologies have been developed in recent years, such as robot navigation, preoperative 3D CT planning, and 3D-guided plate navigation [33], [34], [37]. However, most of these techniques primarily focus on planning the screw entry point and the final position after implantation, as well as evaluating the deviation between the planned and actual trajectories. They do not consider whether the screw is implanted into regions with optimal bone density.

1.4 Research Objectives

Based on the technical challenges associated with CBT screw placement and the limitations identified in existing literature regarding manual surgical planning, this study establishes the following specific research objectives:

1. **To develop a robust optimization framework that automatically determines the optimal CBT entry points and trajectories for each vertebra bilaterally using CT imaging, based on CT-derived bone density distribution, with particular emphasis on the lumbar spine.** The system will optimize key parameters—including the entry point, cranial–caudal and medial–lateral insertion angles, screw diameter, and screw length—for CBT fixation at each vertebral level.

   This optimization process will be guided by patient-specific CT imaging data and will incorporate the following key criteria:

   - Maximization of cortical bone engagement: The algorithm will quantitatively assess and maximize the contact between the screw thread and high-density cortical bone along the entire trajectory, thereby enhancing fixation strength, particularly in osteoporotic patients where cortical bone preservation is critical.
   - Accommodation of anatomical variability: The system will account for inter-

doi:10.6342/NTU202604598

individual and inter-level variations in pedicle morphology, vertebral dimensions, and cortical bone distribution, enabling truly personalized surgical planning rather than relying on population-averaged anatomical assumptions.

- Bone quality consideration: The algorithm will utilize CT-derived bone density information (Hounsfield Units) to differentiate between cortical and cancellous bone regions, preferentially directing screw trajectories through zones of higher bone mineral density to optimize biomechanical purchase.

2. **To develop a comprehensive and intuitive 3D visualization system that effectively translates the computational optimization results into clinically actionable information for surgeons.** By providing clear and real-time visual feedback on the planned screw trajectories, the system aims to assist surgical planning, improve screw placement accuracy, and reduce the risk of complications through enhanced preoperative decision-making. This platform will provide:
    - Interactive 3D anatomical rendering: High-fidelity three-dimensional reconstruction of patient-specific vertebral anatomy from CT imaging, allowing surgeons to visualize bone structures, optimal screw trajectories, and spatial relationships between implants and critical structures.
    - Real-time trajectory simulation: Dynamic visualization of the proposed CBT screw path, including entry point location, angulation in multiple anatomical planes, and predicted cortical bone contact zones, enabling surgeons to evaluate and validate the planned trajectory before surgical execution.
    - Quantitative surgical parameters: Clear presentation of optimized screw dimensions (diameter and length), insertion angles, and bone density metrics along the proposed trajectory, providing objective data to support clinical decision-making.

doi:10.6342/NTU202604598

3. **To validate the clinical utility and performance of the proposed system.**

   A critical objective is to rigorously evaluate the accuracy, reliability, and clinical applicability of the automated optimization algorithm through:

   - Computational validation: Assessment of algorithm performance across a diverse dataset of lumbar spine CT scans, including evaluation of consistency, reproducibility, and sensitivity to variations in imaging quality and anatomical pathology.
   - Comparison with conventional planning: Quantitative comparison of the proposed automated approach against traditional manual surgical planning methods in terms of cortical bone engagement, safety margin adequacy, and screw placement accuracy.
   - Clinical feasibility assessment: Evaluation of the system's practical utility in real-world surgical planning workflows, including analysis of computational efficiency, ease of use, and potential for integration into existing clinical protocols.

Overall Goal and Expected Impact

The overarching goal of this research is to develop a simple and clinically practical automated system that determines optimal cortical bone trajectory (CBT) screw entry points and trajectories for each vertebra—particularly the lumbar spine—using preoperative CT imaging. By incorporating patient-specific anatomical characteristics and CT-derived bone density distribution, the proposed system aims to provide objective, quantitative, and personalized optimization of CBT screw placement, thereby overcoming the limitations of experience-dependent manual planning.

This automated planning framework is designed to enhance surgical precision by

doi:10.6342/NTU202604598

generating optimized screw paths that maximize cortical bone engagement while minimizing anatomical risks, ultimately improving fixation strength and reducing placement errors. Through intuitive visualization and streamlined computational guidance, the system is expected to reduce technical barriers, enabling less experienced surgeons to achieve accuracy comparable to experts and supporting wider clinical adoption of CBT techniques across diverse surgical environments.

By providing objectively optimized screw trajectories based on patient-specific anatomical and bone density information, the system aims to improve patient safety by reducing the incidence of screw-related complications, including pedicle breaches, nerve root injury, screw loosening, and construct failure. In addition, by establishing a reproducible and evidence-based method for CBT trajectory determination, the framework supports standardized surgical planning and reduces inter-operator variability, contributing to more consistent and high-quality surgical outcomes.

Ultimately, this research seeks to advance personalized, image-guided spine surgery by enabling individualized screw trajectory planning tailored to each patient's anatomy and bone quality. The successful development and clinical implementation of this automated CBT optimization system has the potential to improve patient outcomes, reduce operative time, lower complication and revision surgery rates, enhance cost-effectiveness, and advance the state of the art in computer-assisted spinal fusion surgery.

doi:10.6342/NTU202604598

1.5 Novelty of the Study

This research presents several significant novel contributions that distinguish it from existing literature in the field of computer-assisted spinal surgery and cortical bone trajectory screw optimization. The key innovative aspects of this study are outlined as follows:

1. Focus on the emerging cortical bone trajectory technique

While the majority of existing computational planning tools and optimization algorithms for spinal surgery have focused exclusively on traditional trajectory (TT) for traditional transpedicular screw (TPS) placement, this study specifically targets the cortical bone trajectory (CBT) technique—a relatively novel and technically demanding approach introduced only within the past decade and a half. Despite the demonstrated biomechanical advantages and clinical benefits of CBT, particularly in osteoporotic patients and minimally invasive procedures, the technique has not been extensively investigated from a computational optimization perspective.

The unique geometric characteristics of CBT—including its medial-to-lateral and caudal-to-cephalad trajectory, reliance on cortical bone engagement rather than cancellous bone purchase, and distinct entry point locations—necessitate fundamentally different optimization strategies compared to traditional pedicle screw planning. This study addresses this critical gap by developing specialized algorithms tailored to the specific anatomical constraints and biomechanical objectives of CBT screw placement, thereby contributing novel methodological approaches for an underexplored but clinically important surgical technique.

doi:10.6342/NTU202604598

2. First application of Particle Swarm Optimization (PSO) to spinal screw trajectory planning

To the best of our knowledge, this study represents the first application of Particle Swarm Optimization (PSO) algorithms to the problem of surgical screw trajectory optimization in spine surgery. While various computational approaches have been previously applied to surgical planning—including anatomical templating, geometric constraint-based methods, and basic optimization techniques—PSO has not been utilized in this specific clinical domain despite its proven effectiveness in solving complex, multi-objective optimization problems in other engineering and medical applications.

PSO offers several distinct advantages that make it particularly well-suited for CBT screw trajectory optimization:

- **Multi-objective optimization capability:** PSO can simultaneously optimize multiple competing objectives, such as maximizing cortical bone contact while minimizing proximity to critical anatomical structures, without requiring explicit weighting schemes or simplification of the objective function.
- **Global search efficiency:** Unlike gradient-based optimization methods that may converge to local optima, PSO's population-based search strategy explores the solution space more comprehensively, increasing the likelihood of identifying globally optimal or near-optimal screw trajectories.
- **Robustness to complex constraints:** PSO can effectively handle the irregular, non-linear geometric constraints imposed by patient-specific vertebral anatomy, including complex pedicle morphologies, cortical bone distributions, and safety boundaries.
- **Computational efficiency:** PSO's parallel evaluation of multiple candidate solutions enables relatively fast convergence compared to exhaustive search or

doi:10.6342/NTU202604598

iterative single-point optimization methods, making it practical for clinical workflow integration.

- **Flexibility and adaptability:** The PSO framework can be readily adapted to incorporate different optimization criteria (e.g., bone density thresholds, the range of position) or extended to other vertebral levels and screw techniques, providing a versatile platform for future research.

3. Integration of bone density-driven optimization with CT-based segmentation

Unlike previous approaches that primarily rely on geometric or anatomical landmarks for screw trajectory determination, this study incorporates quantitative bone density information derived from CT Hounsfield Unit (HU) values directly into the optimization process. By generating distinct binary masks for cortical bone regions based on density thresholding, the proposed algorithm can explicitly target trajectories that maximize engagement with high-density cortical bone—the fundamental biomechanical principle underlying CBT's advantages over traditional techniques.

This density-driven optimization approach enables:

- Patient-specific adaptation to varying bone quality, particularly relevant for osteoporotic patients
- Quantitative assessment of expected fixation strength based on cortical bone contact
- Objective differentiation between optimal and suboptimal trajectories based on bone tissue characteristics rather than solely geometric criteria

By introducing PSO to the domain of spinal screw placement optimization, this study not only addresses the specific clinical need for automated CBT planning but also

doi:10.6342/NTU202604598

establishes a novel methodological paradigm that could potentially be extended to other surgical planning challenges in orthopedic and neurosurgical procedures.

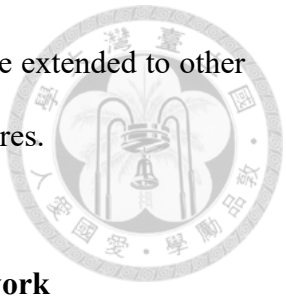

4. Comprehensive bilateral and multi-level optimization framework

The proposed system is designed to simultaneously optimize CBT screw trajectories for bilateral placement across all vertebrae, particularly the lumbar spine (L1–L5), accounting for the anatomical coupling and biomechanical interactions between left and right screws as well as between adjacent vertebral levels. This holistic approach represents an advancement over single-screw or single-level planning methods, providing a more clinically realistic and practically useful surgical planning tool.

doi:10.6342/NTU202604598

Chapter 2 Theoretical Background

2.1 Fundamentals of Medical Image Analysis

Medical image analysis is a foundational component in modern computer-assisted diagnosis and surgical planning [1]. It involves the acquisition, processing, interpretation, and quantitative evaluation of medical images, enabling clinicians and researchers to extract meaningful anatomical and pathological information. Among the various imaging modalities, computed tomography (CT) plays a crucial role due to its high spatial resolution, rapid acquisition speed, and ability to visualize fine structural details, especially within bony anatomy. Effective analysis of CT images typically requires a series of computational steps, including preprocessing, enhancement, segmentation, and feature extraction. These processes provide structured information that supports downstream tasks such as 3D reconstruction, biomechanical modeling, and trajectory optimization in surgical navigation systems.

2.1.1 CT Image Processing

CT image processing encompasses a collection of techniques designed to refine image quality and prepare data for quantitative analysis. Raw CT images often exhibit noise, intensity inhomogeneity, and variations caused by acquisition parameters or patient-specific factors. Therefore, preprocessing steps such as resampling, denoising, intensity normalization, and artifact reduction are commonly applied. In this research, the preprocessing stage consisted of two key operations: resampling the images to a uniform resolution and applying affine standardization. These steps ensured consistent spatial geometry and orientation across all samples, forming a reliable basis for the subsequent segmentation and analysis tasks.

doi:10.6342/NTU202604598

Resampling is particularly important when integrating heterogeneous datasets, as CT images can vary in voxel spacing. Converting all images to a uniform resolution enables consistent geometric interpretation and ensures compatibility with algorithms that rely on spatial precision, such as 3D registration or trajectory computation. In addition, filtering techniques—such as Gaussian smoothing or anisotropic diffusion—can be employed to suppress noise while preserving structural boundaries. These steps collectively establish a reliable foundation for segmentation and subsequent anatomical modeling.

1. Data Format and Acquisition: NIFTI (.nii.gz)

The standard data format for volumetric medical images in research is the NIFTI (Neuroimaging Informatics Technology Initiative) file, typically compressed as .nii.gz. This format is crucial as it consolidates the entire 3D scan into a single file and includes essential metadata (like voxel spacing and orientation) required for subsequent volumetric analysis and optimization tasks.

- Structure: A NIFTI file contains both the image data (as a multi-dimensional array, usually 3D for a single CT scan) and the metadata in a unified header.
- Python Handling: The nibabel library in Python is the standard tool for interacting with NIFTI files. It enables easy loading of the file into a NumPy array for processing while preserving critical header information.

```python
import nibabel as nib

# Load the NIFTI file
nii_img = nib.load('0001.nii.gz')

# Extract the image data as a NumPy array
image_data = nii_img.get_fdata()
```

Fig. 4 Python implementation for loading NIFTI (.nii.gz) using the nibabel library.

doi:10.6342/NTU202604598

2. Image Pre-processing Pipeline

Raw CT data must undergo several essential preprocessing steps to ensure consistency and optimal feature representation for the optimization algorithm.

A. Hounsfield Unit (HU) Processing and Normalization:

CT images are recorded in Hounsfield Units (HU), representing tissue radio-density.

- **Intensity Clipping (Windowing):** To concentrate the analysis on specific tissues (e.g., bone or soft tissue), HU values are clipped to a defined window $[HU_{min}, HU_{max}]$.
- **Normalization:** The clipped data is then normalized (e.g., scaled to the [0, 1] range) to ensure all input data features fall within a consistent numerical magnitude, which is beneficial for the stability and convergence of optimization algorithms like PSO.

B. Resampling and Spacing Unification

CT scans are frequently anisotropic (unequal voxel dimensions). Consistency in the spatial domain is vital for any subsequent analysis.

- **Resampling:** To eliminate directional bias, the volumes must be resampled to a uniform isotropic spacing (e.g., $1\,\text{mm} \times 1\,\text{mm} \times 1\,\text{mm}$ or $0.5\,\text{mm} \times 0.5\,\text{mm} \times 0.5\,\text{mm}$). Libraries such as SimpleITK in Python are commonly used for robust, interpolation-based resampling operations.

C. Affine Registration and Orientation Standardization

After resampling, the CT volume still retains its original orientation, coordinate axes, and anatomical alignment, which may differ across scans. To ensure that all volumes are represented in a consistent spatial framework, an affine transformation is applied. An affine transformation is a 12-parameter linear

doi:10.6342/NTU202604598

mapping that allows translation, rotation, scaling, and shearing of the 3D volume. In the context of medical imaging, affine registration serves two primary purposes:

- **Orientation Standardization:** Medical images obtained from different scanners or institutions may store axes in varying orders (e.g., LPS vs. RAS conventions). Affine alignment reorients all CT volumes to a unified anatomical coordinate system, ensuring that the superior–inferior, anterior–posterior, and left–right directions are consistent across patients.
- **Spatial Alignment:** Although global anatomical variation exists between patients, an affine transformation allows correction of global shifts and rotations, placing the volume into a common reference space. This standardization is essential for any algorithm that relies on spatial reasoning—such as computing entry points, orientations, and possible collision boundaries for screw trajectory planning.

In this research, affine transformations are applied after resampling to guarantee that all subjects share the same coordinate orientation and global alignment. This ensures that subsequent optimization of the screw trajectory is based on anatomically consistent and comparable spatial data across the entire dataset.

2.1.2 Segmentation

Segmentation is the process of delineating specific anatomical structures or regions of interest within medical images. In CT-based musculoskeletal research, segmentation is essential for isolating vertebrae, cortical bone regions, or pathological structures. Accurate segmentation allows for the construction of patient-specific 3D models, quantitative morphological analysis, and precise geometric measurements that guide clinical decision-making.

doi:10.6342/NTU202604598

Segmentation methods range from classical image-processing approaches—such as thresholding, morphological operations, and region growing—to advanced machine learning and deep learning techniques. Traditional methods are computationally efficient but may struggle with complex anatomical variations or ambiguous boundaries. In contrast, modern deep learning models, including convolutional neural networks (CNNs) and transformer-based architectures, provide higher accuracy and robustness by learning hierarchical features directly from imaging data.

Regardless of the technique, segmentation quality has a direct impact on all downstream analyses. Errors or inaccuracies can propagate into biomechanical simulations, navigation planning, or screw trajectory optimization, ultimately influencing the safety and reliability of clinical applications. Therefore, segmentation remains a critical step in medical image analysis pipelines, warranting careful design, validation, and quality control.

2.2 Principles of Image-Based Surgical Planning

Image-based surgical planning refers to the use of pre-operative medical images—typically CT or MRI—to analyze patient-specific anatomy and to design an optimal surgical strategy before the procedure begins. Unlike intra-operative navigation systems, which guide surgeons in real time, image-based planning focuses on generating precise geometric and anatomical information that supports decision-making during surgery.

The foundation of surgical planning is the acquisition of high-resolution, quantitatively reliable imaging data, with CT being the modality of choice for bony structures such as the vertebrae. After image acquisition, computational processing methods such as resampling, affine alignment, and segmentation are applied to

doi:10.6342/NTU202604598

standardize the imaging space and isolate anatomical regions of interest. These preprocessing steps ensure that subsequent geometric analysis is consistent and reproducible across patients.

A key component of image-based planning is the extraction of patient-specific anatomical constraints. In spinal instrumentation, this includes vertebral dimensions, pedicle morphology, cortical boundaries, and proximity to neural structures. These features define feasible screw trajectories and provide safety margins for avoiding cortical breach. By integrating geometric modeling and anatomical measurements, the planning system identifies candidate trajectories that maximize bone purchase while respecting anatomical limits.

Furthermore, computational models allow for the simulation of multiple potential trajectories, enabling quantitative comparison based on metrics such as bone density distribution, cortical contact, or path length. This is particularly valuable in techniques such as the cortical bone trajectory (CBT), where slight adjustments in entry point or angle can significantly influence surgical outcomes.

Overall, image-based surgical planning enhances surgical precision by providing objective, patient-specific information prior to the procedure. As imaging resolution, computational tools, and automated analysis methods continue to improve, pre-operative planning is becoming increasingly quantitative and predictive, laying a solid foundation for safer and more consistent surgical interventions.

doi:10.6342/NTU202604598

2.3 Particle Swarm Optimization (PSO)

Particle Swarm Optimization (PSO) is a population-based stochastic optimization technique inspired by the social behavior of bird flocking or fish schooling [39]. There are various optimization algorithms based on swarm intelligence (SI) with animal behavior, and PSO is one of the most well-regarded swarm-based algorithms. In PSO, each particle in the swarm represents a candidate solution, which moves through the search space guided by its own experience and that of neighboring particles. PSO is particularly effective for nonlinear, non-differentiable, and high-dimensional optimization problems. The algorithm iteratively updates particles' velocities and positions to converge toward optimal solutions based on defined fitness functions.

Due to the collective behavior of the swarm, PSO can mitigate the problem of falling into local minima compared to traditional optimization methods. This characteristic makes PSO suitable for complex and non-convex optimization problems commonly encountered in computational research.

In PSO, each candidate solution is represented as a particle within a multi-dimensional search space. A swarm consists of multiple particles, each of which “flies” through the search space by iteratively updating its position, representing a potential solution, and its velocity, determining the direction and magnitude of movement.

Each particle evaluates the objective function at its current position and retains:

- **Personal best position ($\boldsymbol{pbest}$)** – the best solution the particle has encountered.
- **Global best position ($\boldsymbol{gbest}$)** – the best solution identified by the entire swarm.

The velocity update rule governs exploration and exploitation:

$$v_i^{(t+1)} = wv_i^{(t)} + c_1 r_1 \left(pbest_i - x_i^{(t)}\right) + c_2 r_2 \left(gbest - x_i^{(t)}\right)$$

$$x_i^{(t+1)} = x_i^{(t)} + v_i^{(t+1)}$$

doi:10.6342/NTU202604598

where

- w is the inertia weight controlling momentum,
- c_1 and c_2 are cognitive and social coefficients,
- $r_1, r_2 \sim U(0,1)$ are random factors ensuring stochasticity.

At the end of each iteration, the personal best (***pbest***) and the global best (***gbest***) solutions are updated for the current population. Each particle maintains a record of the best solution it has achieved so far, known as its personal best (***pbest***). In contrast, the global best (***gbest***) refers to the best solution found by any particle in the entire swarm across all generations. The gbest guides the swarm toward promising regions in the search space, while the pbest helps each particle to exploit its own best-found positions, ensuring a balance between exploration and exploitation during the optimization process.

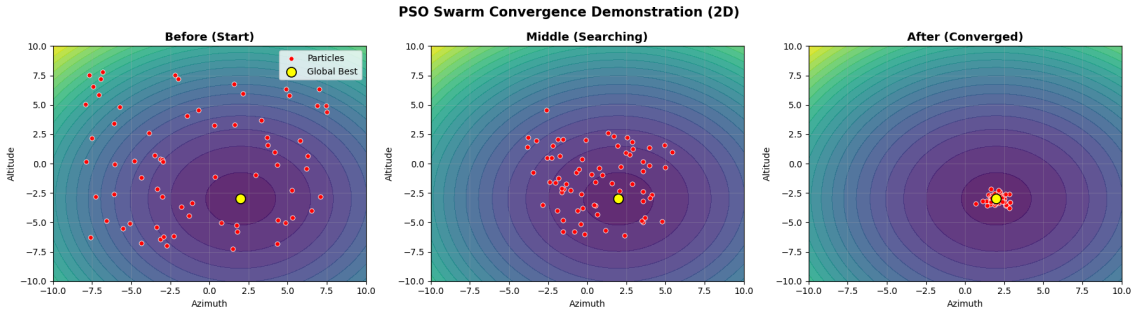

Fig. 5 2D particle swarm optimization visualization

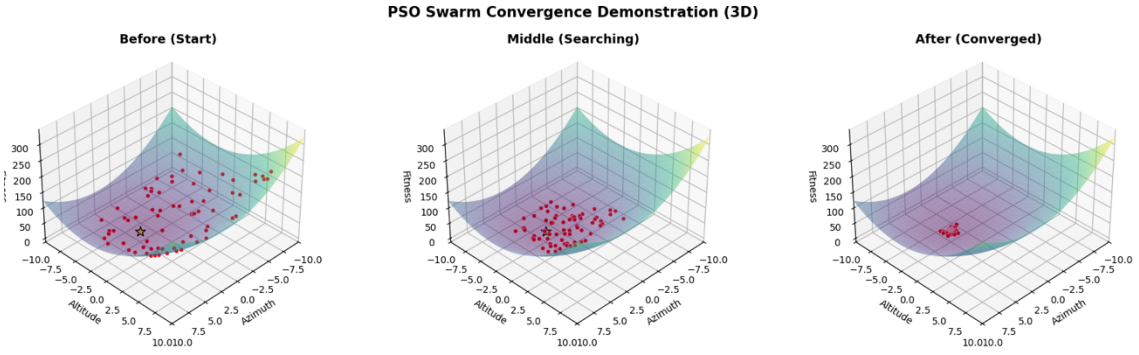

Fig. 6 3D particle swarm optimization visualization

doi:10.6342/NTU202604598

PSO is widely used across engineering and medical applications due to its:

- **Simplicity** – the algorithm is easy to implement and requires few parameters.
- **Continuous optimization capability** – suitable for problems with nonconvex, differentiable or non-differentiable landscapes.
- **Fast convergence** – the swarm quickly identifies promising regions of the search space.
- **Derivative-free nature** – ideal for objective functions where gradients are unavailable (e.g., medical image–based metrics).

These features make PSO highly suitable for optimizing geometric, spatial, or anatomical parameters in medical imaging tasks.

2.4 Comparative Optimization Algorithms

To evaluate the effectiveness of the proposed optimization framework for cortical bone trajectory (CBT) screw planning, a classical derivative-free optimization algorithm, the Powell method, implemented in the SciPy.optimize.minimize function, was adopted as a baseline comparative approach.

The Powell method is a deterministic, direction-set based optimization algorithm that iteratively searches along conjugate directions without requiring gradient information. This characteristic makes it well suited for the present problem, in which the objective function is highly nonlinear, computationally expensive, and may not be differentiable with respect to certain geometric parameters, such as screw angles and entry locations. By successively performing one-dimensional line searches along multiple directions, the Powell algorithm gradually refines the solution toward a local minimum [40].

In this study, the Powell method was applied to optimize the same set of parameters as the proposed framework, including the CBT entry point, insertion angles (cranial–

doi:10.6342/NTU202604598

caudal and medial–lateral), screw diameter, and screw length. All optimization experiments were initialized using identical parameter ranges and boundary conditions to ensure a fair and consistent comparison. The performance of the Powell-based optimization was evaluated in terms of convergence behavior, computational efficiency, and resulting objective function values.

By comparing the proposed optimization framework against the Powell method, this study aims to demonstrate the advantages of the proposed approach in terms of solution quality, stability, and applicability to patient-specific CBT planning.

2.5 PyTorch Framework

PyTorch is an open-source machine learning framework that provides efficient tensor computation and automatic differentiation capabilities, and it has become a widely adopted platform for scientific computing, medical image analysis, and optimization-based learning systems. One of the key advantages of PyTorch is its dynamic computational graph mechanism, which allows model structures and optimization processes to be defined and modified at runtime. This feature is particularly advantageous for complex geometric optimization problems such as CBT trajectory planning, where the objective function involves non-linear spatial relationships, conditional constraints, and iterative evaluation of candidate solutions.

In this study, PyTorch serves as the core computational backbone for implementing and accelerating the proposed optimization framework. All geometrical computations, including CBT entry point parameterization, screw trajectory generation, and objective function evaluation, are formulated using PyTorch tensor operations. This tensor-based formulation enables efficient batch-wise evaluation of multiple candidate solutions in

doi:10.6342/NTU202604598

parallel, which is essential for population-based optimization algorithms such as particle swarm optimization (PSO). By leveraging PyTorch's native support for vectorized computation, the computational cost associated with repeated trajectory evaluation and scoring can be significantly reduced.

Another critical advantage of PyTorch is its built-in support for GPU acceleration. By transferring large-scale tensor operations to the GPU, the system achieves substantial improvements in computational efficiency, particularly when handling high-resolution three-dimensional CT volumes and dense sampling of CBT trajectories. This capability is crucial for maintaining practical execution time in patient-specific optimization tasks, where repeated forward evaluations of complex geometric models are required. The use of GPU acceleration also enables scalable expansion of the optimization framework to larger search spaces and higher-resolution anatomical representations without prohibitive increases in runtime.

Although the present framework primarily employs derivative-free optimization strategies (e.g., PSO and Powell's method), PyTorch's automatic differentiation engine provides important extensibility for future integration of gradient-based optimization and learning-based approaches. This design choice ensures that the proposed system is not limited to the current optimization paradigm but can be readily extended to hybrid optimization-learning frameworks, including deep reinforcement learning or differentiable anatomy-based cost functions.

In addition, PyTorch provides a flexible and modular software architecture that facilitates rapid prototyping, debugging, and future system expansion. The seamless integration with Python-based scientific libraries allows efficient interfacing with CT image processing, geometric modeling, and visualization modules. Collectively, these advantages make PyTorch a robust and scalable computational platform for the

doi:10.6342/NTU202604598

implementation of the proposed automated CBT optimization system.

2.6 Bresenham's Line Algorithm

Bresenham’s line algorithm is a classical rasterization algorithm that determines the discrete grid points intersected by a straight line between two locations in a grid-based space using only integer arithmetic. Owing to its computational efficiency, numerical robustness, and deterministic behavior, the algorithm has been widely adopted in computer graphics and volumetric image analysis for voxel traversal and collision detection tasks.

In this study, Bresenham’s line algorithm is specifically employed as a geometric intersection detection tool to verify the anatomical feasibility of simulated CBT screw trajectories within three-dimensional CT image volumes. Given a continuous screw axis defined by the optimized entry point and trajectory direction, the algorithm generates a voxel-wise digital representation of the line path. Along this path, binary intersection states between the screw trajectory and the segmented vertebral bone are evaluated.

To ensure safe screw placement, the number of intersections between the simulated trajectory and the cortical bone boundary is explicitly constrained. Specifically, a valid CBT screw trajectory is required to exhibit no more than two intersections with the bone surface—corresponding to one entry and one exit point through the cortical shell. Trajectories that exhibit more than two intersections are classified as cortical breach events, indicating unintended screw penetration outside the bony envelope and are therefore rejected as anatomically invalid solutions.

This intersection-based validation mechanism enables efficient and objective detection of screw perforation without the need for computationally expensive surface

doi:10.6342/NTU202604598

mesh collision modeling. By operating directly on voxelized CT representations, the Bresenham-based traversal ensures consistent and reproducible intersection testing across all candidate trajectories. This feature is particularly important in large-scale optimization settings, where thousands of simulated screw paths must be evaluated repeatedly under varying geometric configurations.

Moreover, the deterministic nature of Bresenham's algorithm guarantees identical voxel traversal paths for identical trajectory inputs, thereby preserving the numerical stability and repeatability of the feasibility assessment across different optimization runs and algorithmic comparisons. As a result, the algorithm serves as a reliable geometric constraint validation module within the proposed CBT optimization framework.

In summary, within this study, Bresenham's line algorithm functions not merely as a discretization tool, but as a core anatomical feasibility validator that enables rapid identification of cortical breaches and ensures that only physically plausible screw trajectories are retained for subsequent optimization and clinical interpretation.

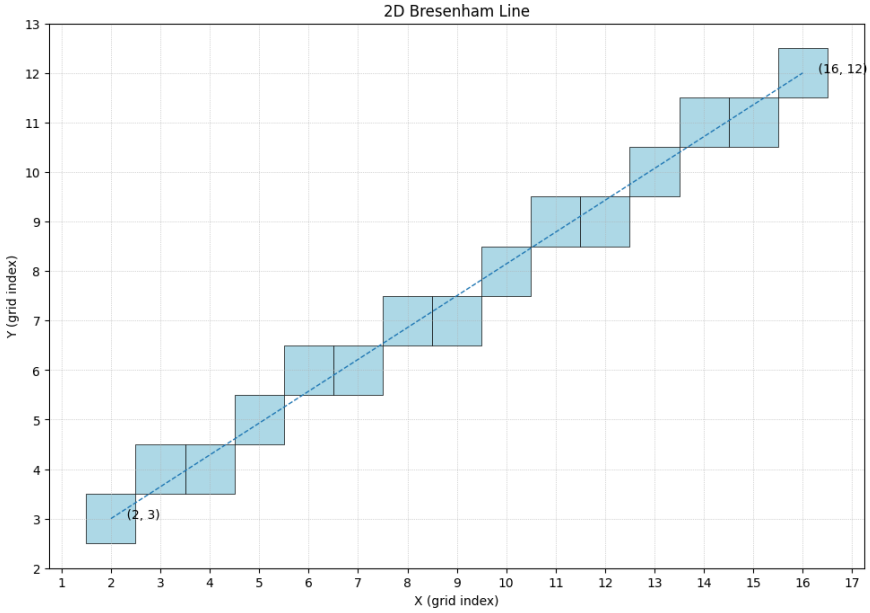

Fig. 7 2D bresenham line

doi:10.6342/NTU202604598

Chapter 3 Methodology

We utilized the publicly available CTSpine1K [38] dataset, which provides large-scale and comprehensive spinal images, to obtain volumetric CT scans of the lumbar spine. From each scan, we extracted individual vertebrae using pre-existing segmentation labels. Preprocessing was performed to ensure spatial consistency, without applying any image enhancement techniques. Specifically, we standardized the voxel spacing and aligned the orientation of each volume using an affine transformation to enforce a consistent anatomical direction.

3.1 CTSpine1K Dataset

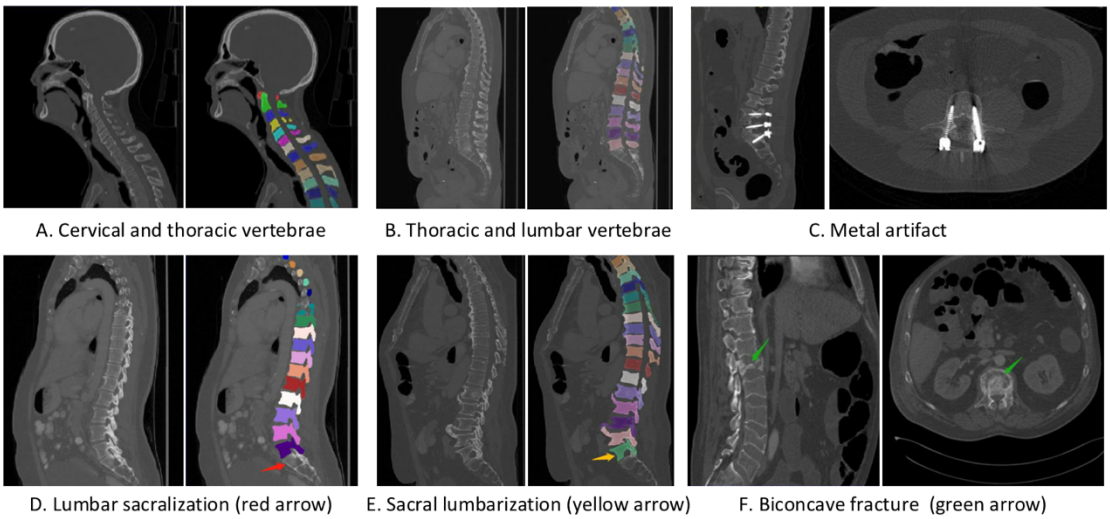

Fig. 8 Examples of CTSpine1K dataset (adapted from [38]).

This study employs the CTSpine1K dataset, a large-scale and publicly accessible collection of annotated spinal CT scans designed to support research in vertebral analysis and computer-assisted spine surgery. The dataset contains 1,005 clinical CT volumes, curated from four open-source repositories to capture a wide range of anatomical diversity,

doi:10.6342/NTU202604598

imaging conditions, and patient demographics. In total, CTSpine1K provides over 500,000 labeled axial slices and more than 11,000 expert-annotated vertebrae, covering levels from C1 through L5.

Each CT volume in the dataset is accompanied by corresponding vertebral labels, enabling accurate identification of spinal levels and facilitating downstream tasks such as segmentation, landmark localization, and spatial analysis. The dataset exhibits substantial heterogeneity in vertebral morphology, pedicle dimensions, curvature severity, degenerative changes, and bone quality, making it a realistic representation of clinical variations encountered in spinal imaging.

In the context of this work, CTSpine1K serves as an external validation resource for evaluating the robustness and generalizability of the proposed CBT trajectory optimization framework. The large sample size and diverse anatomical patterns allow systematic assessment across different spinal levels and morphologies. Specifically, CTSpine1K enables the examination of algorithm performance under variations in vertebral size, pedicle shape, cortical bone distribution, and overall structural complexity—factors that are critical for clinically meaningful CBT planning. Only intact and fully annotated vertebrae were included in the evaluation to ensure consistency and anatomical completeness during trajectory analysis.

The use of CTSpine1K provides a standardized benchmark for trajectory optimization research and ensures that the proposed system is tested across a wide anatomical spectrum, thereby enhancing its potential for real-world clinical translation.

CTSpine1K is composed of four publicly sourced sub-datasets, each contributing different anatomical characteristics, imaging protocols, and demographic variations:

doi:10.6342/NTU202604598

1. **COLONOG**: Derived from the CT COLONOGRAPHY trial, this subset includes 825 DICOM-format abdominal CT scans. For each patient, one of two available scan positions was randomly selected. Because abdominal scans typically capture the lower thoracic and lumbar region with high anatomical completeness, this subset provides the most reliable coverage of the **L1–L5 vertebrae**, making it particularly suitable for lumbar-focused evaluation in this study.
2. **HNSCC-3DCT-RT**: This subset contains high-resolution head-and-neck CT scans (pre-, mid-, and post-treatment) acquired with a Siemens 16-slice CT scanner. The images focus primarily on the cervical region and therefore provide limited lumbar information.
3. **MSD T10 (Medical Segmentation Decathlon Task 03 – Liver)**: Although this dataset includes 201 abdominal CT scans in NIfTI format, the visibility of spinal levels varies considerably. Lumbar vertebrae may not always be fully captured due to field-of-view differences.
4. **COVID-19**: This subset contains 40 non-enhanced chest CT scans in NIfTI format. These scans predominantly cover thoracic anatomy and rarely include the lumbar spine.

Among the four sub-datasets included in CTSpine1K, the COLONOG subset is the only one that consistently contains full coverage of the lumbar spine (L1–L5). Because the scans originate from abdominal CT colonography studies, the field of view naturally encompasses the entire lumbar region. In contrast, the cervical (C) and thoracic (T) vertebrae in COLONOG are not always fully visible or completely annotated, as they often fall outside the primary imaging range.

doi:10.6342/NTU202604598

Given that the primary objective of this research is to evaluate automated CBT planning at the lumbar vertebral levels, the COLONOG subset was selected as the main dataset for quantitative analysis. Its reliable and complete lumbar coverage ensures that all L1–L5 vertebrae required for this study are available, whereas inconsistent visibility of C and T levels renders them unsuitable for lumbar-focused experimentation.

To further substantiate the selection of the COLONOG subset, we conducted a comprehensive census of the annotated vertebral levels across the dataset. The resulting distribution, summarized in the statistics below, quantitatively confirms the high consistency of lumbar annotations compared to the sparser coverage in the cervical and thoracic regions.

As evidenced by the data summarized in Table 1, the lumbar vertebrae (L1–L4) exhibit a 100% presence rate (n=784), with L5 appearing in 98.9% of the scans (n=775). In stark contrast, the occurrence of cervical vertebrae is negligible, and the upper thoracic levels (T1–T5) remain significantly underrepresented. This empirical evidence validates that the COLONOG subset provides a robust and near-complete anatomical representation of the lumbar spine, satisfying the requirements for reliable Cortical Bone Trajectory (CBT) planning analysis.

Although a negligible number of cervical vertebrae (C1 and C6) were initially identified, further inspection revealed that these instances represented incomplete anatomical coverage at the peripheral margins of the field of view. Consequently, these cervical levels provided insufficient volumetric data for reliable 3D reconstruction and were thus excluded from the subsequent analysis.

doi:10.6342/NTU202604598

Table 1 Statistical distribution of annotated vertebral levels in the COLONOG subset (N=784).

Region	Vertebral Level	Frequency (n)
Cervical	C1	2 (0.3%)
	C2	0
	C3	0
	C4	0
	C5	0
	C6	2 (0.3%)
	C7	0
Thoracic	T1	0
	T2	0
	T3	1 (0.1%)
	T4	9 (1.1%)
	T5	33 (4.2%)
	T6	150 (19.1%)
	T7	328 (41.8%)
	T8	532 (67.9%)
	T9	675 (86.1%)
	T10	748 (95.4%)
	T11	780 (99.5%)
	T12	783 (99.9%)
Lumbar	L1	784 (100%)
	L2	784 (100%)
	L3	784 (100%)
	L4	784 (100%)
	L5	775 (98.9%)

doi:10.6342/NTU202604598

3.2 Proposed Algorithm

In this study, the COLONOG subset of the CTSpine1K dataset was used as the primary data source, as it provides complete coverage of all lumbar vertebrae (L1–L5). Based on the provided vertebral labels, each lumbar segment was first isolated through label-based segmentation. Following segmentation, a preprocessing pipeline was applied, consisting of resampling and affine normalization. The CT volumes were resampled to an isotropic resolution of $0.5\,\text{mm} \times 0.5\,\text{mm} \times 0.5\,\text{mm}$ to preserve fine anatomical details relevant to screw insertion. Affine normalization was then performed to standardize orientation across all vertebrae and ensure consistency in subsequent analysis.

After preprocessing, a binary mask was generated for each isolated vertebra to define the region of interest (ROI). This step prepares the data for efficient geometric evaluation by representing the vertebral structure as a binary voxel grid. Although the detailed processing of bone density–based enhancement will be discussed in the next section, the purpose of this step is to enable more accurate assessment of screw feasibility, including the determination of optimal entry points, insertion angles, screw length, and screw diameter according to the 3D vertebral morphology.

To simulate screw placement, each candidate CBT screw was modeled as a cylindrical object. The screw diameter and length were selected from discrete, clinically feasible sets, with diameters of $\{3.5, 4.0, 4.5, 5.0\}$ mm and lengths of $\{35, 40, 45, 50\}$ mm. In total, seven parameters were optimized using Particle Swarm Optimization (PSO):

- **diameter:** the screw diameter (discrete),
- **length:** the screw length (discrete),
- **x, y, z**: the screw entry point coordinates,
- **azimuth**: the rotational angle in the horizontal plane,

doi:10.6342/NTU202604598

- **altitude**: the rotational angle in the vertical plane.

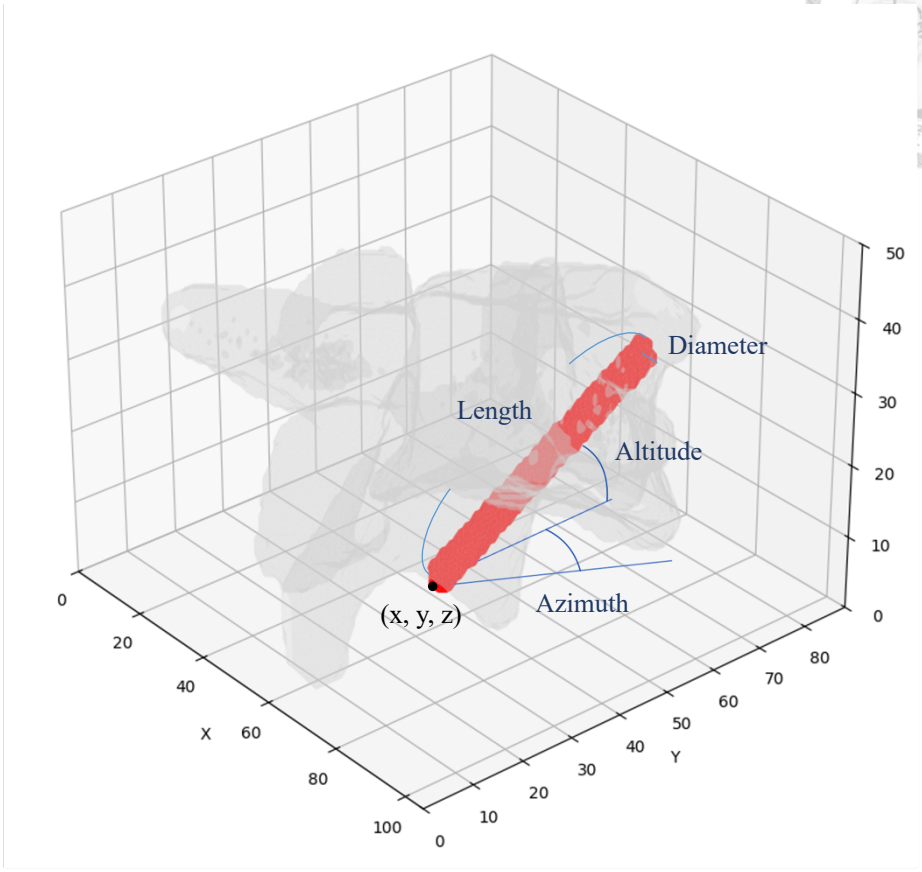

Fig. 9 Illustration of the seven parameters optimized in the PSO framework.

Given a candidate parameter set, the corresponding cylinder was generated and evaluated against the binary mask. Overlapping voxels between the screw model and the vertebral mask were assigned positive scores, representing stable screw engagement with cortical and cancellous bone. Voxels falling outside the mask indicated cortical breach or extraosseous placement and were penalized.

To further ensure anatomical validity, Bresenham's line algorithm was applied to the central axis of the simulated cylinder. By tracing this discrete line through the binary mask, the number of intersections with the vertebral boundary was computed. A valid CBT trajectory should produce no more than two intersection points (entry and exit through

doi:10.6342/NTU202604598

cortical bone). Any trajectory exceeding two intersections indicates screw perforation or an unintended breach, which results in additional penalization.

PSO was then used to search for the optimal parameter combination $(diameter, length,\ x, y, z, azimuth, altitude)$ that maximizes screw stability while respecting anatomical constraints. Through iterative refinement, the algorithm identifies the most suitable entry point and trajectory for each lumbar vertebra.

doi:10.6342/NTU202604598

3.3 A Projection-Based Approach for Calculating Vertebral Orientation

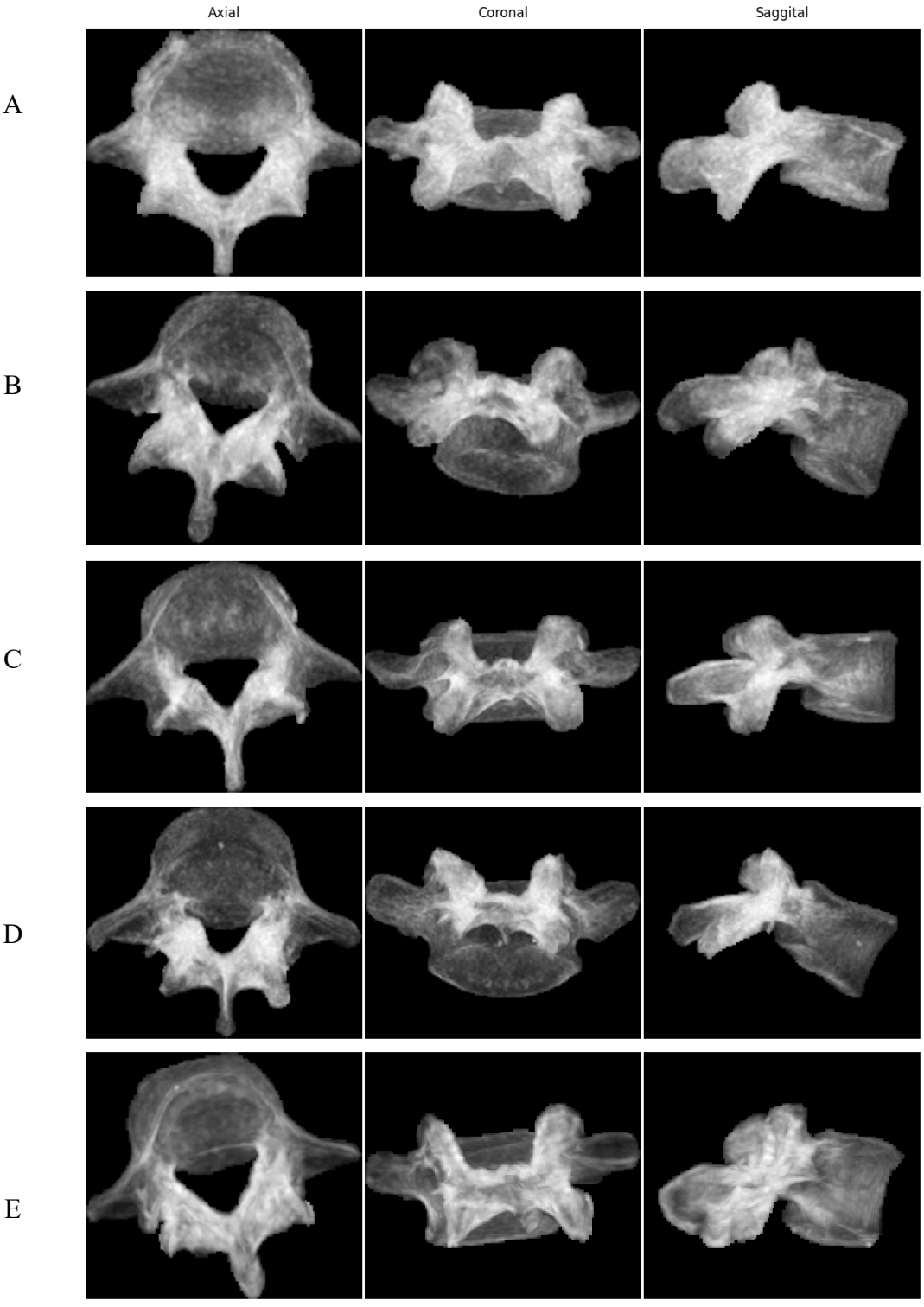

Fig. 10 Examples of segmented L5 vertebrae from five patients.

doi:10.6342/NTU202604598

Before defining the azimuth and altitude angles for CBT trajectory planning, it is important to note that vertebral orientation in medical images is not inherently standardized.

Although CT volumes are acquired in a nominal anatomical coordinate system, variations in patient positioning, spinal curvature, and post-processing during segmentation often introduce residual rotational and tilt deviations in the extracted vertebral masks.

Fig. 10 illustrates inter-subject variability in vertebral orientation, including differences in axial rotation and sagittal tilt, which motivates the need for geometry-based azimuth and altitude calibration.

As a result, the same vertebra may appear upright in one case but noticeably tilted or rotated in another, even after rigid alignment of the image volume. If such orientation differences are not explicitly addressed, CBT trajectories defined in the image coordinate system may no longer correspond to consistent anatomical directions, leading to biased angle initialization and reduced reproducibility across subjects.

To overcome this limitation, we introduce a geometry-driven calibration framework that estimates the azimuth and altitude angles directly from vertebral morphology.
By aligning trajectory orientation with intrinsic anatomical features rather than the raw image axes, the proposed method provides a robust and patient-specific reference for CBT planning.

doi:10.6342/NTU202604598

3.3.1 Azimuth

The three-dimensional vertebral segmentation was first projected along the superior–inferior axis using a maximum intensity projection, yielding a binary axial projection. The centroid of all foreground pixels (c_x, c_y) was computed to represent the geometric center of the vertebral body in the axial plane.

To estimate the dominant vertebral orientation, the most anterior row of foreground pixels in the projection was identified. The median x-coordinate of this row was selected as a representative boundary point (x_t, y_t). A direction vector $\vec{v}$ was then defined from this anterior boundary point to the centroid:

$$\Delta x = c_x - x_t, \qquad \Delta y = c_y - y_t$$

Considering the downward orientation of the image y-axis, the axial rotation angle was computed using the two-argument arctangent function:

$$\theta_{\text{azimuth}} = \arctan\ 2(\Delta x, \Delta y)$$

This angle represents the deviation of the vertebral long axis from the reference y-axis in the axial plane and was used as the **azimuth calibration angle** for CBT trajectory planning. By estimating the orientation from intrinsic anatomical geometry, this step minimizes systematic errors introduced by patient pose or scanner alignment.

doi:10.6342/NTU202604598

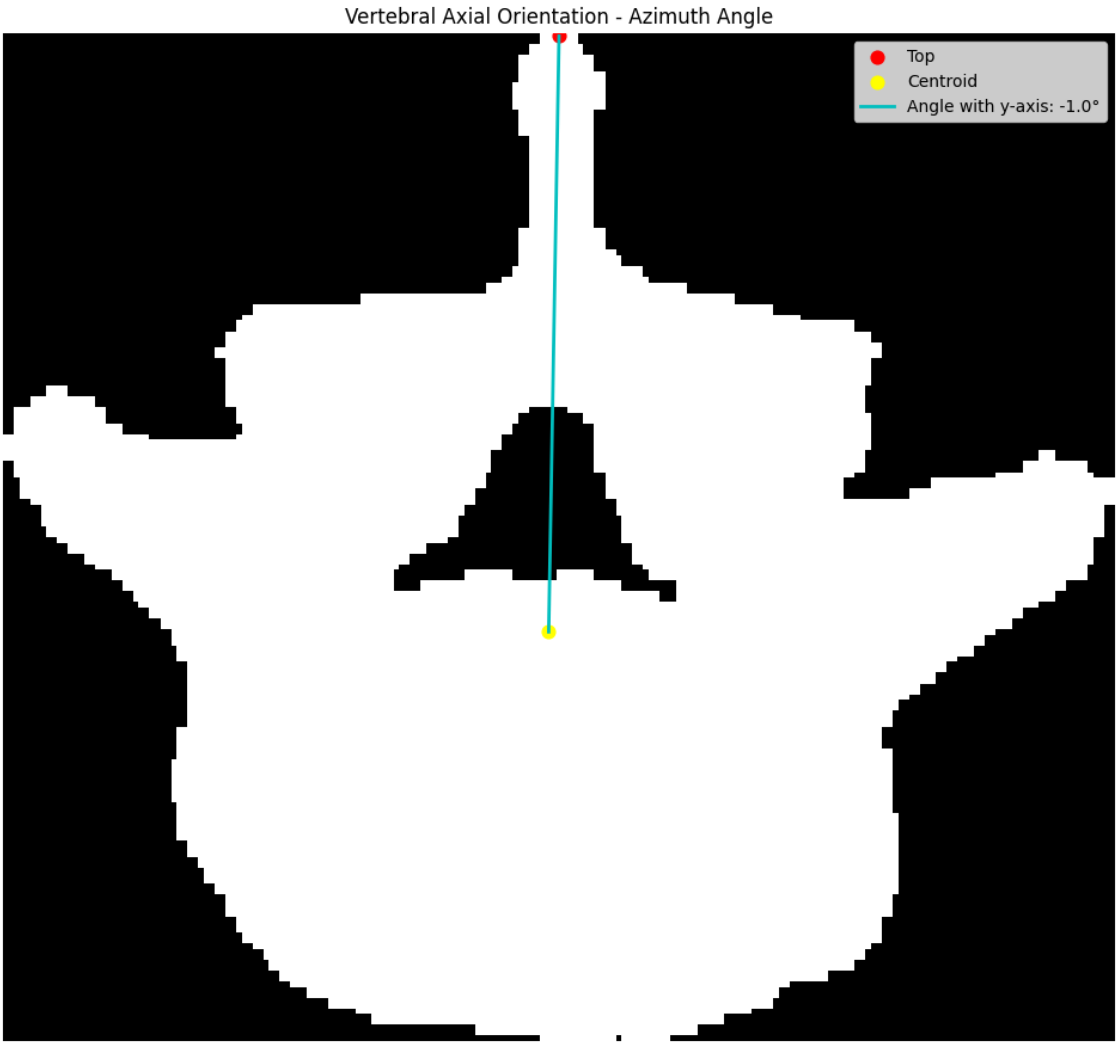

Fig. 11 Estimation of vertebral axial orientation using the top-point–centroid axis

In the axial view, the vertebral orientation is estimated by the inclination of the line connecting the topmost boundary point of the projected contour and the geometric centroid, measured with respect to the image y-axis.

doi:10.6342/NTU202604598

3.3.2 Altitude

To estimate sagittal alignment, the segmentation volume was projected along the left–right axis to generate a sagittal binary projection. Based on the projection centroid, the vertebral region was divided into anterior and posterior halves, and only the anterior portion was retained for endplate analysis in order to reduce interference from posterior elements such as pedicles and laminae.

For each sagittal slice, boundary points of the vertebral body were extracted, and the contours of the superior and inferior endplates were constructed. To achieve robustness against segmentation noise and local irregularities, RANSAC-based linear regression was applied to fit a straight line to each endplate contour while automatically rejecting outliers.

Let m denote the slope of the fitted endplate line. The sagittal tilt angle was then computed as:

$$\theta_{\text{altitude}} = \arctan(m)$$

This angle characterizes the anterior–posterior inclination of the vertebral body in the sagittal plane and serves as the altitude calibration angle for CBT trajectory definition. The coefficient of determination (R^2) and the number of inliers were additionally recorded to quantify fitting reliability.

doi:10.6342/NTU202604598

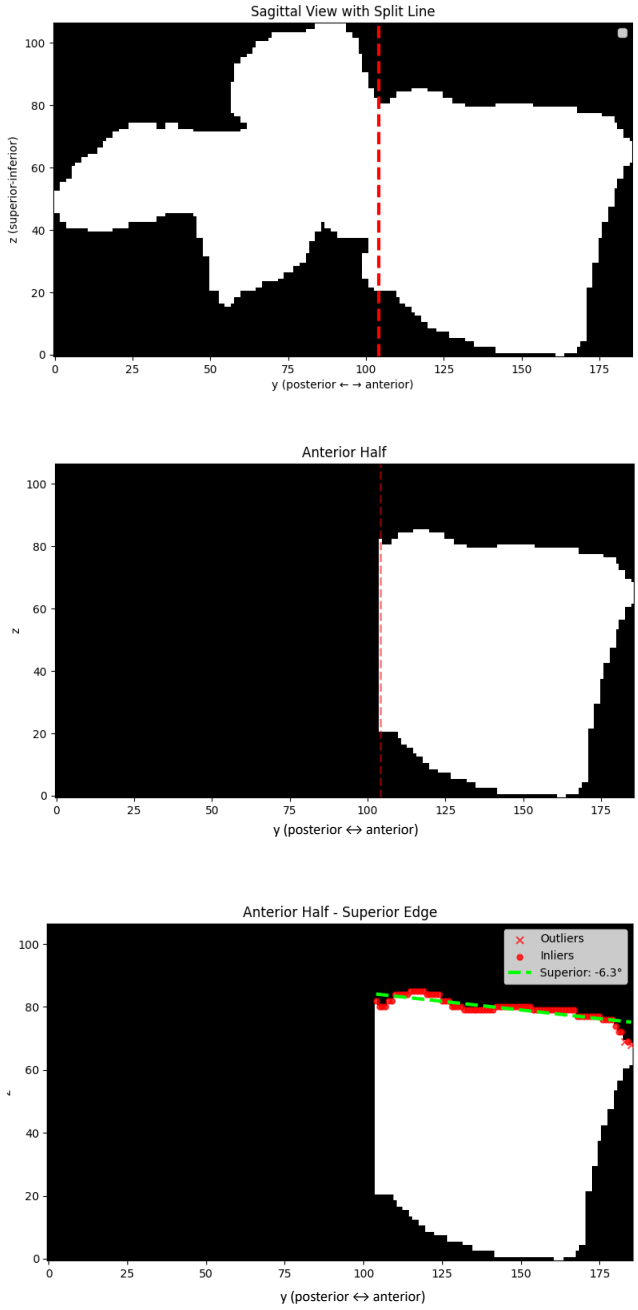

Fig. 12 Estimation of vertebral sagittal orientation for altitude angle determination.

Through this two-stage calibration process, the azimuth angle captures the intrinsic axial rotation of the vertebra, whereas the altitude angle reflects its sagittal inclination. Together, these angles provide a patient-specific orientation reference that aligns CBT trajectories with the actual anatomical posture rather than the fixed image coordinate system.

doi:10.6342/NTU202604598

This calibration strategy improves the robustness and reproducibility of trajectory planning across patients and imaging protocols, and enhances the clinical interpretability of CBT screw orientation in relation to vertebral anatomy.

3.4 Vertebral ROI Extraction and HU-based Bone Characterizationration (Thresholding methods)

To support geometric evaluation and optimization of screw trajectories, two types of binary masks were generated from each preprocessed vertebra. These masks serve complementary analytical purposes: the bone mask defines the anatomical boundary of the vertebra, while the cortical-oriented mask highlights regions of presumed cortical bone based on relative intensity distribution in Hounsfield Units (HU). The details of each mask construction process are described below.

3.4.1 Bone Mask Generation

The bone mask is a binary representation of the complete vertebral structure. A fixed-intensity threshold was applied to each CT volume to differentiate bone tissue from surrounding soft tissue and background. Voxels with intensity values exceeding the predetermined threshold were assigned a value of 1, while all other voxels were set to 0, yielding a binary image that captures the full three-dimensional geometry of the vertebra.

This mask is essential for tasks that require defining the anatomical boundaries of the vertebra, such as:

- evaluating whether a simulated screw lies within the vertebral body,
- detecting cortical breaches,
- restricting optimization search space to feasible anatomical regions.

The bone mask ensures that all computations involving screw overlap or

doi:10.6342/NTU202604598

containment are consistently referenced to the vertebra's true spatial extent.

Binary masks were generated using the anatomical labels provided by the CTSpine1K dataset. Each vertebra is assigned a unique label index; in the lumbar region, the mapping is defined as L1 = 20, L2 = 21, L3 = 22, L4 = 23, and L5 = 24.

To isolate a target vertebra, a binary mask was first created by applying a thresholding operation `BinaryThreshold` to the label volume using SimpleITK. For example, to extract the L5 vertebra, voxels with label value 24 were assigned a value of 1, while all other voxels were set to 0:

binary1 = BinaryThreshold(label, lowerthreshold=24, upperthreshold=24)

This operation yielded a vertebra-specific binary mask defining the anatomical region of interest.

The resulting mask was then multiplied with the corresponding CT volume to obtain a vertebra-only CT image in which voxels outside the target vertebra were set to zero while the original Hounsfield Unit (HU) values within the vertebra were preserved. This step ensured that all subsequent intensity-based analyses were restricted to the anatomical extent of the selected vertebra.

To generate the final bone mask, a second thresholding operation was applied within the vertebral ROI. Voxels with HU values exceeding a predefined bone threshold were classified as bone tissue and assigned a value of 1, whereas all remaining voxels were set to 0. This process produced a binary bone mask representing the three-dimensional geometry of the vertebra.

The bone mask serves as a fundamental anatomical reference in the proposed framework. It is used to determine whether simulated screw trajectories remain within the vertebral body, to detect potential cortical breaches, and to constrain the optimization search space to anatomically feasible regions.

doi:10.6342/NTU202604598

3.4.2 Cortical-Oriented Mask Generation

In addition to the bone mask, a cortical-oriented mask was generated to approximate regions of higher-density cortical bone. Instead of applying a fixed global HU threshold—which may not generalize well across patients, scanners, or vertebral levels—this mask was derived using an adaptive, vertebra-specific strategy based on the relative HU distribution within each segmented vertebra.

For each vertebra, the median HU value was first computed from the vertebra-specific CT region of interest (ROI). Voxels with intensities above this median value were classified as cortical-oriented regions and assigned a value of 1, whereas voxels below the median were assigned a value of 0. This procedure yields a binary mask that emphasizes relatively high-density bone structures within each individual vertebra.

In implementation, the same SimpleITK-based approach described in Section 3.4.1 was utilized. After extracting the vertebra-specific CT ROI by masking the original CT volume with the dataset-provided segmentation labels, a cortical-oriented binary mask was created by applying the previously described thresholding operation to the ROI image using the subject-specific median HU value as the lower bound. Voxels with HU values greater than or equal to the median were assigned to the cortical-oriented class, while all remaining voxels were excluded.

This adaptive thresholding strategy offers two major advantages:

1. **Personalized cortical estimation:** It accounts for inter-patient variability and local anatomical differences in bone density.
2. **Robustness across vertebral levels:** Median-based separation avoids the instability of fixed thresholds in the presence of noise, scanner differences, or varying bone quality.

doi:10.6342/NTU202604598

The resulting cortical-oriented mask is subsequently used in the scoring of candidate screw trajectories during optimization. Regions with higher HU—presumed to represent mechanically stronger cortical tissue—are assigned greater weight to encourage trajectories that maximize cortical engagement and potentially improve fixation strength.

After defining this cortical-oriented region of interest, the distribution of HU values within the vertebra is further analyzed to establish a quantitative basis for bone-quality–aware CBT trajectory evaluation, as described in Section 3.4.3.

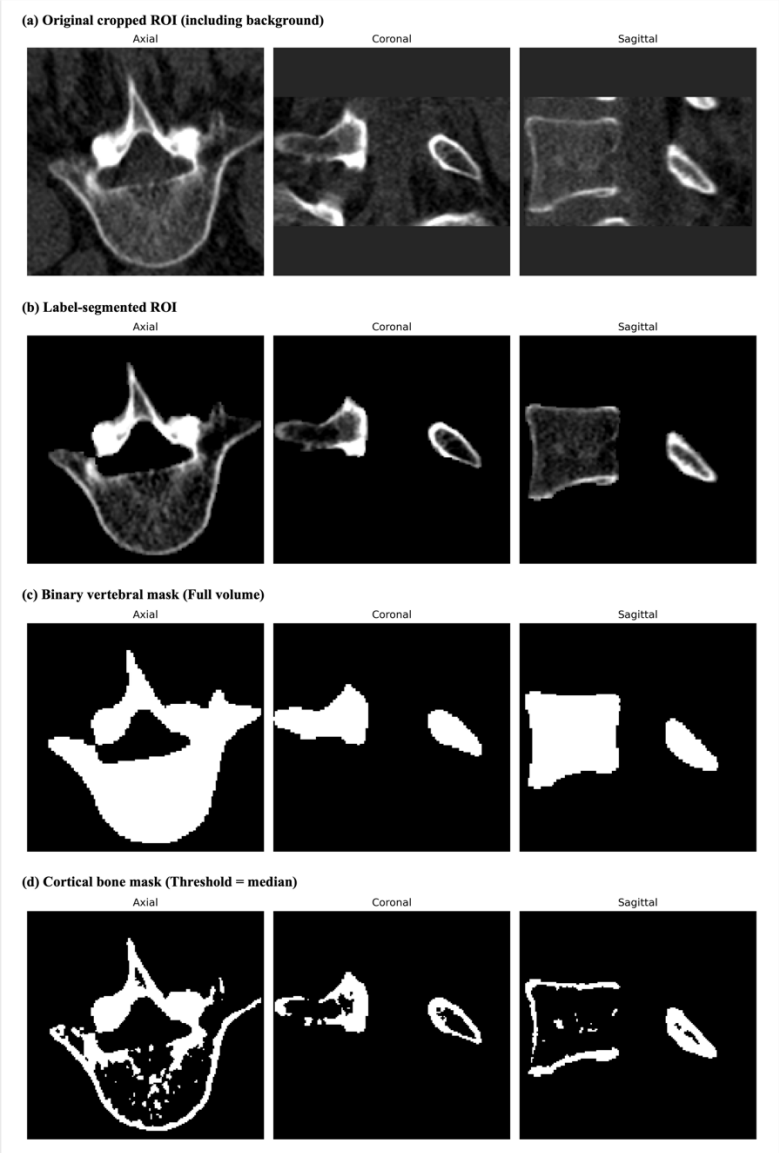

Fig. 13 **Visualization of the preprocessing and mask generation pipeline for the L5 vertebra.** (a) Original ROI: The initial cropped region containing the patient's L5 vertebra,

doi:10.6342/NTU202604598

including the surrounding anatomical background. (b) Segmented ROI: The isolated L5 region obtained after background removal using label-based segmentation, focusing strictly on the vertebral structure. (c) Binary Bone Mask: A complete binary representation of the ROI where all internal pixels are assigned a value of 1. This mask serves as a geometric template for the entire vertebra, independent of specific Hounsfield Unit (HU) thresholds. (d) Cortical Bone Extraction: The final mask generated by applying an adaptive threshold based on the median HU value (in this case, median = 308 HU). Only pixels within the ROI exceeding this threshold are retained to represent the higher-density cortical bone structures.

3.4.3 HU-based Bone Density Interpretation

After generating the bone mask and the cortical-oriented region of interest, the distribution of Hounsfield Units (HU) within the vertebral ROI was analyzed to characterize local bone density and to support bone-quality–aware CBT trajectory evaluation. Standard window width and level settings (e.g., soft tissue: W = 250, L = 50; bone: W = 1800, L = 400) are widely adopted for visualization; however, all quantitative analyses in this study are performed using the underlying HU values rather than windowed intensities.

Although intensity clipping and normalization are applied in the general image preprocessing pipeline to ensure numerical stability for optimization, all bone density analyses in this study are performed using the original HU values to preserve their physical meaning. HU statistics are computed exclusively within the segmented vertebral ROI, thereby excluding background structures, air, and surrounding soft tissues that may otherwise bias intensity-based measurements.

doi:10.6342/NTU202604598

For each subject, descriptive statistics including the minimum, maximum, mean, median, standard deviation, and selected percentiles (5th, 25th, 75th, and 95th) of HU values were calculated. The median HU typically fell within the range associated with cancellous bone, reflecting the volumetric dominance of trabecular structures within the vertebral body, whereas higher-percentile values captured the presence of dense cortical regions that are mechanically critical for screw fixation.

To provide a robust and scanner-independent characterization of bone density, HU values within the ROI were further stratified into percentile-based intervals (0–25%, 25–50%, 50–75%, and 75–100%). This relative partitioning enabled consistent comparison of low-, medium-, and high-density osseous regions across subjects without relying on fixed HU thresholds, which may vary due to acquisition protocols and reconstruction parameters.

Importantly, this HU-based interpretation is not used for segmentation itself but serves as a quantitative descriptor of bone quality for subsequent trajectory evaluation. In particular, the distribution of HU values along candidate CBT paths is analyzed to estimate the degree of cortical engagement and to penalize trajectories traversing predominantly low-density regions. Through this strategy, geometric feasibility and bone mechanical relevance are jointly considered in the trajectory planning framework.

Across the cohort of 784 subjects, the median HU value within the vertebral ROI was 280 HU (interquartile range: 249–316 HU), reflecting the volumetric dominance of cancellous bone. In contrast, the median 95th-percentile HU reached 959 HU (interquartile range: 866–1047 HU), confirming the consistent presence of high-density cortical regions across patients. These findings demonstrate that, although low-to-medium density bone constitutes the majority of vertebral volume, dense cortical structures are reliably captured within the ROI, providing a robust basis for bone-quality–

doi:10.6342/NTU202604598

aware CBT trajectory evaluation.

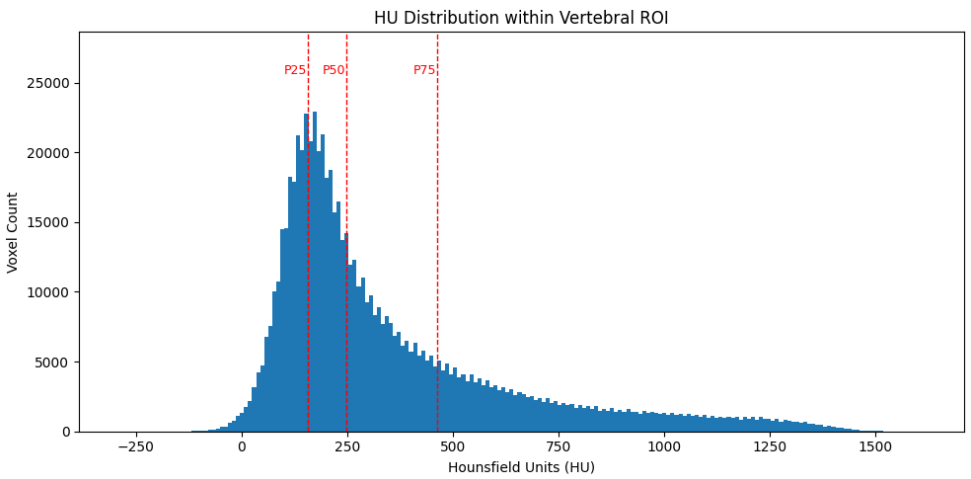

Fig. 14 HU Distribution within the vertebral region-of-interest (ROI) of a representative subject

3.5 Cylindrical Screw Representation

To simulate pedicle screw geometry during trajectory optimization, a three-dimensional cylindrical model was generated directly in voxel space. The cylinder represents a screw with specified diameter, length, spatial position, and orientation, and is encoded as a binary mask aligned with the CT image grid.

Given a screw defined by its diameter d, length L, insertion point (x_0, y_0, z_0), azimuth angle θ, and altitude angle ϕ, a dense 3D coordinate grid was first constructed using PyTorch tensors to match the dimensions of the target volume. All voxel coordinates were translated so that the screw insertion point coincided with the origin of the local coordinate system.

The orientation of the screw was modeled using a two-angle parameterization. The azimuth angle θ defines the rotation in the axial plane, while the altitude angle ϕ controls the cranio–caudal inclination. These angles were converted from degrees to radians and applied through a rotation transformation to the shifted voxel

doi:10.6342/NTU202604598

coordinates, yielding a rotated coordinate system (x', y', z') aligned with the screw axis. We apply a rotation transformation to align the grid with the cylinder's local frame. The rotation matrix R(φ, θ) combines azimuthal and altitudinal rotations:

$$\begin{matrix} x_{rot} \\ (y_{rot}) \\ z_{rot} \end{matrix} = \begin{pmatrix} \cos\phi\cos\theta & \sin\phi\cos\theta & -\sin\theta \\ -\sin\phi & \cos\phi & 0 \\ \cos\phi\sin\theta & \sin\phi\sin\theta & \cos\theta \end{pmatrix} \begin{matrix} x' \\ (y') \\ z' \end{matrix}$$

As a result, a voxel was classified as belonging to the cylindrical screw if it satisfied two geometric conditions:

(1) its radial distance from the screw axis fulfilled

$$x'^2 + y'^2 \leq (\frac{d}{2})^2,$$

and

(2) its axial coordinate lay within the screw length,

$$0 \leq z' \leq L.$$

To ensure compatibility with different image resolutions, voxel spacing was explicitly considered during mask generation. For isotropic spacing of 1 mm, the cylinder dimensions were applied directly. For finer resolutions (e.g., 0.5 mm spacing), both the radius and axial length were scaled accordingly to preserve the physical dimensions of the screw in real space.

The resulting cylinder was stored as a binary mask, where voxels inside the cylinder were assigned a value of 1 and all other voxels were set to 0. This binary representation enables efficient computation of geometric overlap, intersection counts, and intensity-based scoring during optimization. The entire cylinder generation process was implemented using PyTorch to allow efficient tensor operations and seamless integration into the optimization pipeline.

doi:10.6342/NTU202604598

3.6 Objective Fuction Design

To optimize the pedicle screw trajectory using Particle Swarm Optimization (PSO), we designed a multi-objective loss function that balances fixation strength and surgical safety. The screw is modeled as a rigid cylinder, with its trajectory axis computed using a 3D extension of Bresenham's line algorithm to facilitate precise voxel-wise intersection detection.

The scoring mechanism operates on a reward-penalty basis. Fixation quality is quantified by the voxel overlap with the cortical structure. To ensure safety, we incorporate a strict intersection penalty; specifically, any trajectory that penetrates the bone surface more than once—indicating a cortical breach—is heavily penalized. Furthermore, the loss function accounts for the contralateral trajectory to avoid interference with the adjacent spinal anatomy. This formulation transforms the pathfinding problem into a constrained optimization task, guiding the PSO particles toward an anatomically optimal and clinically safe orientation.

The objective function L is formulated to maximize the trajectory quality by considering both anatomical engagement and safety constraints. Let V_{cyl} be the set of voxels occupied by the simulated screw cylinder, $V_{cortical}$ be the cortical bone mask, and V_{spine} represent the entire spinal structure. The loss function is defined as:

$$L = -(\lambda_1 \cdot O_{cortical} - \lambda_2 \cdot E_{ext} - \lambda_3 \cdot E_{opp} - P_{min} - P_{inter})$$

where:

- $O_{cortical} = |V_{cyl} \cap V_{cortical}|$ denotes the volume of overlap between the cylinder and the cortical bone, serving as a reward for structural fixation.
- $E_{ext} = |V_{cyl} \setminus V_{cortical}|$ represents the volume of the cylinder extending beyond the cortical boundary (null voxels), which is penalized to ensure

doi:10.6342/NTU202604598

containment.

- $E_{opp} = |V_{cyl} \cap V_{spine}|$ penalizes the extension of the contralateral cylinder into the spinal structure to prevent encroachment on the opposite segment.
- P_{min} is a step-function penalty applied if the cortical engagement $O_{cortical}$ falls below a functional threshold (T = 100 voxels).
- $P_{inter} = \max(0, N_{inter} - 1) \cdot \omega$ is the intersection penalty, where N_{inter} is the number of intersections between the cylinder axis (generated via Bresenham's algorithm) and the bone surface.

3.7 Implementation Details

All image preprocessing, segmentation, mask generation, and optimization procedures were implemented in Python. Standard scientific computing libraries were used throughout the pipeline, including NumPy for numerical operations, SimpleITK for image loading, resampling, and affine transformation handling, and NiBabel for managing NIfTI image formats and performing affine standardization. Visualization and debugging were conducted using Matplotlib and VTK for 2D and 3D rendering, respectively.

The vertebral-level extraction utilized the provided label maps from the COLONOG subset of CTSpine1K. All images were resampled to an isotropic resolution of $0.5\ \text{mm} \times 0.5\ \text{mm} \times 0.5\ \text{mm}$ to ensure consistent spatial resolution across subjects. Binary masks (bone and cortical masks) were generated through threshold-based methods as described in Section 3.4.

The optimization framework, including the simulation of candidate CBT screw trajectories, voxel-wise cylinder rendering, and score computation, was implemented

doi:10.6342/NTU202604598

using PyTorch to leverage tensor parallelization. GPU acceleration significantly improved computation speed, especially for batch evaluation of multiple candidate trajectories during PSO iterations. All experiments were executed on a workstation equipped with an NVIDIA A40 GPU (48 GB VRAM), an Intel Xeon CPU, and 256 GB of system memory. Floating-point computations were performed using 32-bit precision unless otherwise specified.

doi:10.6342/NTU202604598

Chapter 4 Results

4.1 Sensitivity Analysis of PSO Hyperparameters

To evaluate the influence of PSO hyperparameters on the performance and stability of the proposed optimization framework, we conducted a two-stage sensitivity analysis. For consistency across all experiments, each optimization run generated two CBT trajectories (left and right) on the L5 vertebra using a fixed screw diameter of 5.0 mm and a fixed length of 50 mm. This controlled setup enabled us to isolate and quantify the effects of hyperparameter variations while minimizing confounding factors related to screw geometry.

To systematically evaluate the optimization results, we defined two evaluation metrics as:

$$Cortical\ Bone\ Score = \frac{N_{overlap\ \ cortical}}{N_{total}} \times 100$$

$$Vertebral\ Bone\ Score = \frac{N_{overlap_vertebral}}{N_{total}} \times 100$$

$$Cortical - to - Bone\ Ratio = \frac{Cortical\ Bone\ Score}{Vertebral\ Bone\ Score}$$

where $N_{overlap_cortical}$ is the number of cylinder points that intersect with cortical bone, indicating the degree of cortical engagement, while $N_{overlap_vertebral}$ represents the number of cylinder points that intersect with entire veterbral bone, and N_{total} is the total number of points along the cylinder.

doi:10.6342/NTU202604598

4.1.1 Experimental Setup

To systematically identify the optimal configuration for the proposed Particle Swarm Optimization (PSO) algorithm, a comprehensive grid search was conducted to jointly evaluate the effects of swarm size and iteration count. This strategy allows the interaction between these two key hyperparameters to be examined while revealing the trade-offs between exploration capability, convergence stability, and computational cost.

The swarm size was varied from 50 to 100 particles in increments of 10, while the maximum number of iterations was tested at 100, 120, 140, 150, 160, 180, and 200, resulting in 42 hyperparameter configurations. To account for the stochastic nature of PSO, each configuration was executed three independent times on the L5 vertebra of a representative patient.

Optimization performance was evaluated using three anatomical metrics: the Cortical Bone Score, the Vertebral Bone Score, and the Cortical-to-Bone Ratio. In addition, the total computational time was recorded to assess algorithmic efficiency. The results from the three runs were averaged and visualized as heatmaps, enabling intuitive analysis of the hyperparameter landscape and identification of the most stable and efficient configuration..

4.1.2 Effect of Swarm Size and Iteration Count

As illustrated in the heatmaps (Fig. 15), the three anatomical metrics—Cortical Bone Score, Vertebral Bone Score, and Cortical-to-Bone Ratio—showed only minor variation across the tested hyperparameter grid. The objective scores fluctuated within relatively narrow ranges (approximately 81–85 for the Cortical Bone Score and 91–95 for the Vertebral Bone Score), without demonstrating any consistent or monotonic improvement as either the swarm size or the maximum iteration count increased. This finding suggests

doi:10.6342/NTU202604598

that the proposed PSO framework is relatively robust and insensitive to moderate changes in hyperparameter settings.

In contrast, the average total computational time increased markedly with both swarm size and iteration count. As shown in the time heatmap, runtime scaled from approximately 60 s at the smallest tested configuration (50 particles, 100 iterations) to approximately 246 s at the largest tested configuration (100 particles, 200 iterations), indicating a substantial increase in computational burden.

These results reveal a clear trade-off between computational cost and optimization redundancy: larger swarm sizes and longer iteration schedules substantially increased runtime, yet did not produce meaningful improvements in anatomical fitting performance. Therefore, to achieve an effective balance between efficiency, solution quality, and convergence stability, a swarm size of 70 and a maximum iteration count of 100 were selected for all subsequent experiments. This configuration achieved competitive fitting performance (Cortical Bone Score = 84.82, Vertebral Bone Score = 94.34, Cortical-to-Bone Ratio = 0.90) with stable repeated-run variability (CV < 0.05) in approximately 85 s. The detailed numerical results of all hyperparameter configurations are provided in Appendix.

doi:10.6342/NTU202604598

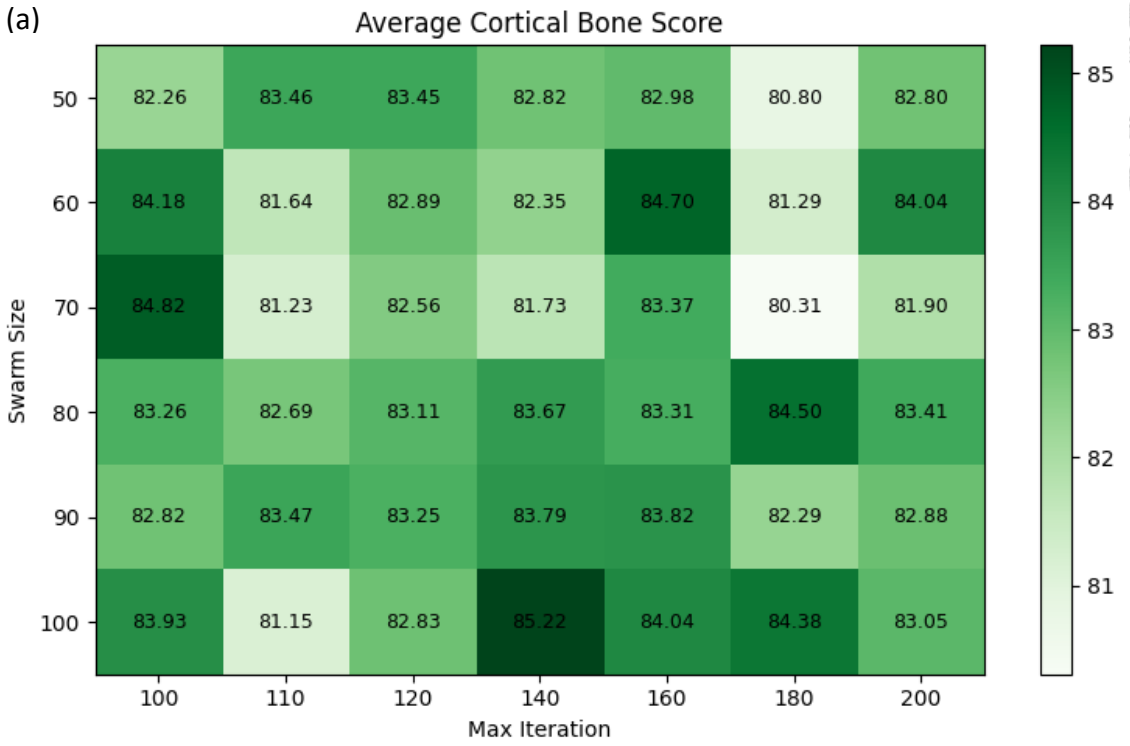

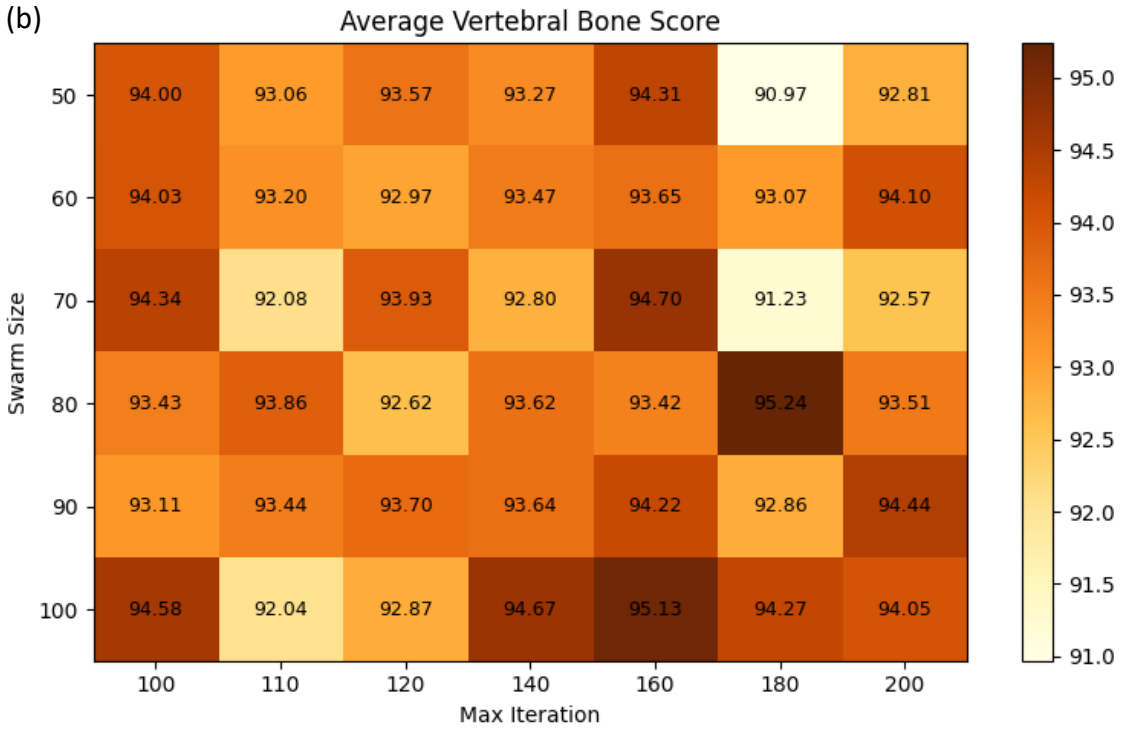

doi:10.6342/NTU202604598

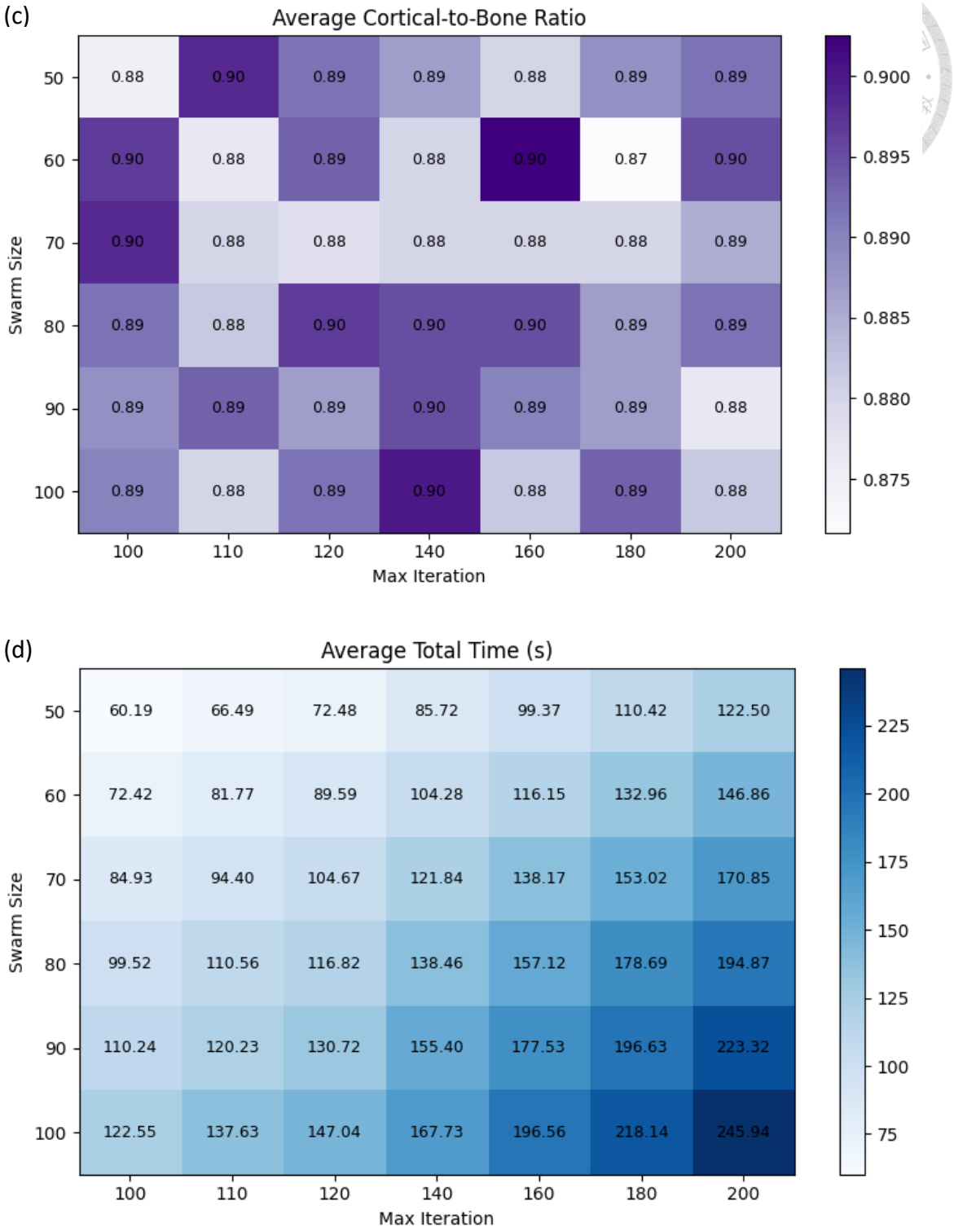

Fig. 15 Heatmaps of the PSO hyperparameter sensitivity analysis. Metrics are averaged over three independent runs: (a) Cortical Bone Score, (b) Vertebral Bone Score, (c) Cortical-to-Bone Ratio, and (d) Total Computational Time (s). The configuration (swarm size = 70, iterations = 100) was selected to balance fitting quality and efficiency.

doi:10.6342/NTU202604598

4.2 Performance Evaluation of the Proposed Method

4.2.1 Iterative Optimization Process of the PSO Algorithm

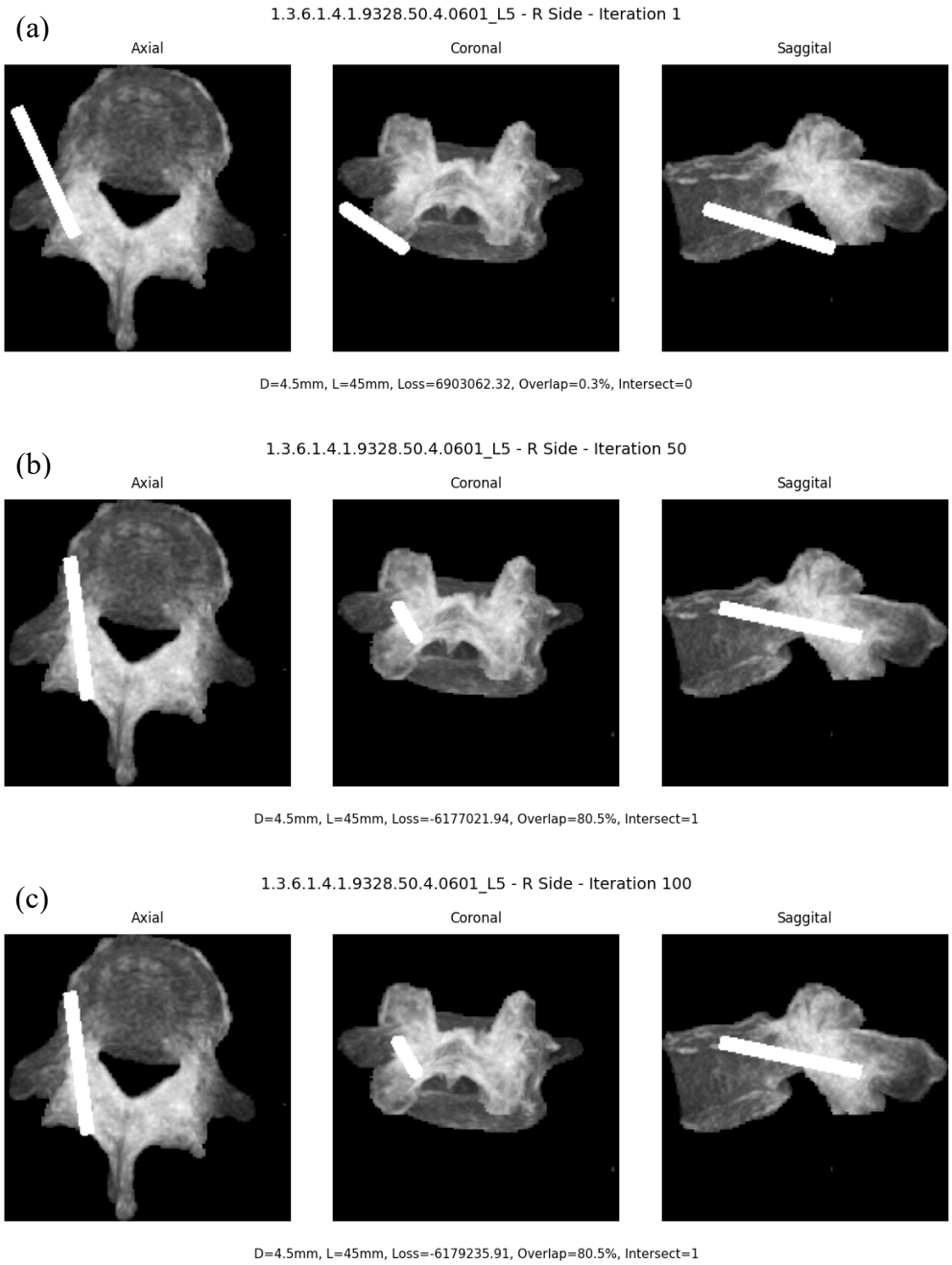

Fig. 16 Snapshots of the screw trajectory optimization process. (a) iteration = 1: Initial random placement with anatomical violations. (b) iteration = 50 : Intermediate refinement as particles move toward the optimal zone. (c) iteration = 100 : Final optimized trajectory with maximal cortical engagement.

doi:10.6342/NTU202604598

The iterative progression of the PSO algorithm is illustrated at three representative stages in Fig. 16. At iteration = 1 (Fig. 16a), the trajectory is initialized with random parameters, often resulting in significant cortical breaches or substantial displacement from the target vertebral region. By iteration = 50 (Fig. 16b), the particle swarm has successfully identified the pedicle canal, significantly reducing the loss value. The final state at iteration = 100 (Fig. 16c) demonstrates a stable and anatomically optimized alignment, confirming the algorithm's ability to converge within a limited number of iterations.

4.2.2 Lumbar Spine Results (L1-L5)

The proposed CBT trajectory planning framework was evaluated on lumbar vertebrae (L1–L5) using the CTSpine1K dataset. For each vertebral level, representative cases are presented to illustrate the geometric feasibility and anatomical consistency of the planned trajectories.

As shown in Fig. 17, the planned trajectories consistently follow a cortical bone trajectory pattern across all lumbar levels. The screw paths remain within the vertebral body and demonstrate appropriate medial–lateral and cranial–caudal orientations, indicating stable geometric performance of the proposed method.

Despite anatomical variations among lumbar levels, including differences in pedicle morphology and vertebral size, the proposed method successfully generated feasible CBT trajectories for all tested levels without requiring level-specific parameter tuning.

In our representative lumbar cases (n = 10), the planned cephalad (altitude) angles ranged from 13.6° to 30.0°, with 4/10 trajectories falling within the commonly reported CBT cephalad range of 25°–30°. Overall, the results demonstrate a clear CBT-like cranial angulation trend consistent with prior descriptions of a 25–26° cephalad orientation.

doi:10.6342/NTU202604598

For the axial-plane orientation, the azimuth values showed the expected left–right symmetry (negative on the left and positive on the right), consistent with the 5 o'clock/7 o'clock directional convention. However, the magnitude of azimuth was generally smaller than the ~30° orientation often implied by the clock-face description, with an average absolute azimuth of approximately 18.3° (range: 11.83°–25.62°). This suggests a relatively conservative medialization, potentially influenced by patient-specific anatomy, image-based landmark definitions, and the optimization weighting that prioritizes breach avoidance and intra-pedicular containment.

These qualitative results demonstrate the general applicability of the proposed framework to lumbar vertebrae with diverse anatomical characteristics, providing a solid basis for the quantitative and comparative analyses presented in the following section.

doi:10.6342/NTU202604598

Table 2 Representative cortical bone trajectory (CBT) planning results for lumbar vertebrae (L1–L5).

	L/R	Diameter (mm)	Length (mm)	Start Point	Azi	Alt	Intersection	Cortical Score	Bone Score	C/B ratio
L1	L	5.0	45	(28.09, 43.50, 60.80)	-24.88	30.00	2	79.83	80.26	99.46
	R	4.5	45	(29.05, 49.20, 92.33)	17.18	27.87	1	75.78	90.89	83.38
L2	L	4.5	40	(38.05, 55.70, 38.07)	-11.83	23.01	1	73.56	92.29	79.71
	R	4.5	40	(33.93, 55.70, 75.20)	16.87	24.87	1	75.94	89.43	84.92
L3	L	5.0	45	(46.14, 73.55, 87.60)	-15.53	16.99	2	80.87	89.05	90.81
	R	5.0	35	(52.16, 77.64, 142.11)	13.93	13.55	1	86.28	96.59	89.33
L4	L	4.5	45	(25.26, 52.62, 73.58)	-20.50	28.06	1	62.13	94.03	66.07
	R	5.0	50	(25.79, 58.50, 110.40)	19.09	29.79	1	84.01	94.13	89.25
L5	L	5.0	40	(38.07, 50.10, 82.00)	-25.62	23.11	1	72.47	99.56	72.79
	R	5.0	45	(34.97, 49.15, 123.00)	17.56	27.56	1	75.28	98.56	76.38

doi:10.6342/NTU202604598

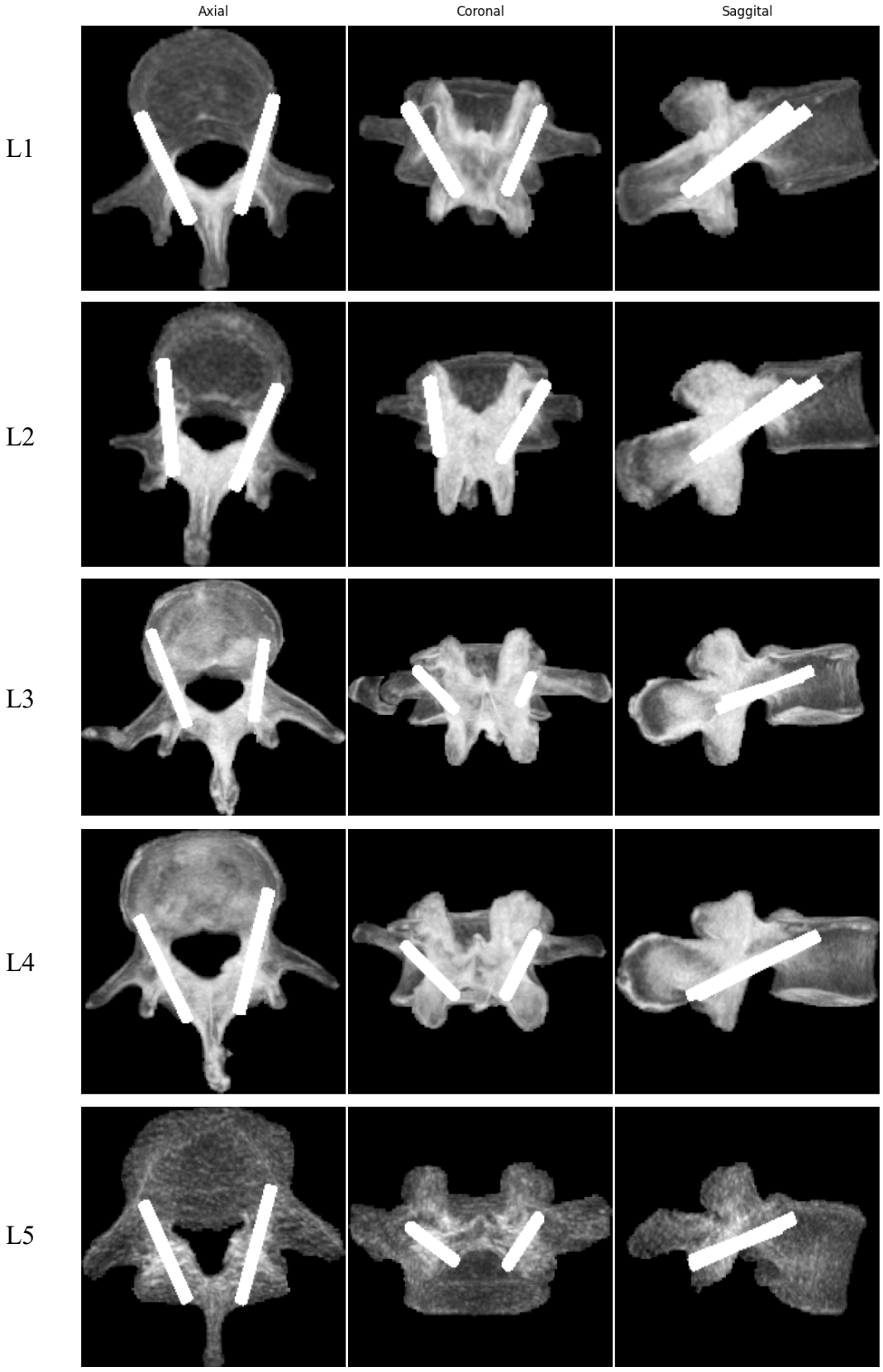

Fig. 17 Representative cortical bone trajectory (CBT) planning results for lumbar vertebrae (L1–L5)

doi:10.6342/NTU202604598

4.3 Comparison with State-of-the-Art

Previous studies on cortical bone trajectory (CBT) planning have primarily relied on rule-based geometric constraints, atlas-based approaches, or deterministic optimization strategies to determine feasible screw paths. While these methods have demonstrated promising results, most of them formulate the problem as a purely geometric task and rarely incorporate bone-quality–aware objective functions into the optimization process.

To the best of our knowledge, this study represents the first attempt to employ Particle Swarm Optimization (PSO) for automated CBT trajectory planning. Unlike conventional deterministic methods, PSO enables an efficient exploration of the high-dimensional parameter space defined by screw position, orientation, and size, allowing the optimization process to escape local optima and to adaptively search for globally favorable solutions. This characteristic is particularly advantageous in CBT planning, where the feasible solution space is highly constrained by complex vertebral anatomy.

In addition, existing approaches typically rely on fixed anatomical landmarks or manually defined regions of interest to approximate cortical bone engagement. In contrast, the proposed framework introduces a cortical-oriented mask derived from the relative HU distribution within each vertebra, which is used as a computational target during trajectory optimization. By explicitly incorporating this mask into the objective function, the optimization process is guided not only by geometric feasibility but also by a quantitative proxy of bone mechanical quality. To the best of our knowledge, this is also the first study to integrate a cortical-oriented mask into an optimization-driven CBT planning framework.

Compared with prior methods that treat cortical engagement as a post hoc evaluation criterion, our approach embeds bone-quality awareness directly into the optimization loop.

doi:10.6342/NTU202604598

This integration allows the algorithm to actively favor trajectories that traverse high-density cortical regions, rather than merely filtering trajectories after geometric planning has been completed.

Overall, the proposed method advances the state of the art in CBT trajectory planning in two fundamental aspects:

(1) it introduces a swarm-intelligence–based optimization strategy to a domain that has traditionally relied on deterministic or heuristic rules; and

(2) it establishes a bone-quality–aware planning paradigm by incorporating a cortical-oriented mask as an explicit optimization target. Together, these contributions provide a new perspective on how anatomical geometry and local bone quality can be jointly considered in automated spinal screw trajectory planning.

doi:10.6342/NTU202604598

Chapter 5 Discussion

5.1 Angular Deviation

A noteworthy observation in this study is that the optimized trajectories occasionally deviate from the commonly cited CBT angular conventions, such as a cephalad angle of 25–30° and the 5 o'clock/7 o'clock axial orientation. While these guidelines have proven valuable in clinical practice, they primarily represent population-level heuristics derived from averaged anatomical characteristics and accumulated surgical experience.

In contrast, the proposed framework formulates CBT planning as a subject-specific optimization problem, in which the optimal trajectory is determined by the combined influence of patient-specific anatomy, local bone density distribution, and safety-related constraints. As a result, the mathematically optimal solution under this formulation does not necessarily coincide with conventional rule-based angles in every case. Rather than indicating a limitation of the proposed method, this deviation highlights the potential of data-driven optimization to move beyond fixed heuristic rules and toward personalized CBT planning strategies that adapt to individual anatomical and mechanical conditions.

5.2 Anatomical Constraints

From an anatomical perspective, the performance of the proposed framework also exhibits a clear dependence on vertebral level. Across the evaluated cases, the most favorable CBT trajectory planning results were consistently observed at the lower lumbar levels, particularly L4 and L5. At these levels, the relatively larger vertebral body and wider pedicle corridor provide a more permissive anatomical environment for trajectory optimization, enabling the algorithm to identify screw paths that achieve both geometric feasibility and substantial cortical engagement.

As the vertebral level ascends from L3 to L1, however, the anatomical constraints

doi:10.6342/NTU202604598

become progressively more restrictive. The pedicles narrow, the vertebral body dimensions decrease, and the available cortical corridors for safe screw insertion are reduced. Under these conditions, identifying an ideal CBT path becomes increasingly challenging. In several upper-level cases, the planned trajectories exhibited minor distal tip breaches, reflecting the inherent difficulty of balancing cortical engagement and breach avoidance within a limited anatomical workspace.

These observations highlight an important interaction between algorithmic optimization and anatomical feasibility. While the proposed method is capable of adapting to diverse vertebral morphologies, its performance is ultimately bounded by the geometric and structural constraints imposed by the anatomy itself. The occasional tip breaches observed in upper lumbar levels should therefore be interpreted not as algorithmic failure, but as an indication of the trade-off between maximizing cortical engagement and maintaining strict containment within narrow pedicle corridors.

The representative examples shown in Fig. 18 illustrate this phenomenon, where lower lumbar trajectories demonstrate stable intraosseous paths, whereas upper-level trajectories occasionally approach or slightly cross the cortical boundary at the distal end. These findings underscore the importance of incorporating level-specific anatomical considerations and adaptive safety margins in future extensions of the framework.

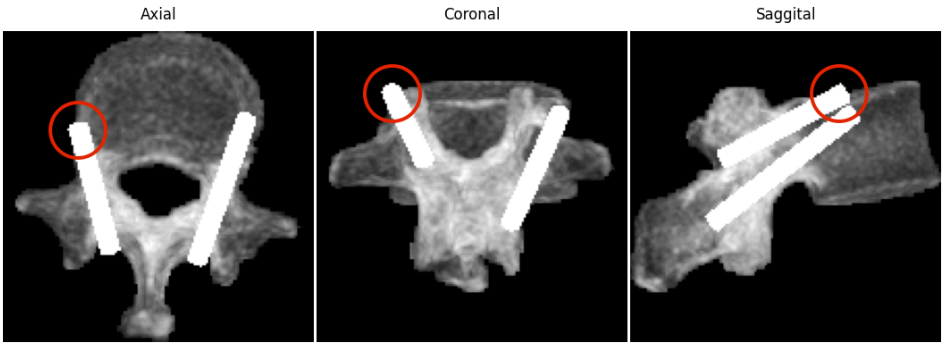

Fig. 18 Representative example of distal tip breach in upper lumbar cortical bone trajectory (CBT).

doi:10.6342/NTU202604598

5.3 Thread Modeling Limitation

In this study, pedicle screw trajectories were modeled using a simplified cylindrical representation. This abstraction was adopted to reduce computational complexity and to allow efficient optimization of screw position and orientation within the vertebral anatomy. However, this modeling approach does not explicitly account for the presence of screw threads, which may influence the mechanical interaction between the screw and surrounding bone tissue.

In clinical practice, pedicle screws are designed with helical threads that enhance fixation strength by increasing the contact area and generating compressive and shear stresses within the bone. The thread geometry plays a significant role in determining pull-out strength, insertion torque, and stress distribution along the screw–bone interface. By contrast, a smooth cylindrical model assumes uniform contact and neglects localized stress concentrations induced by threads, potentially leading to differences between simulated and real-world mechanical behavior.

Despite this limitation, simplified cylindrical or smooth-surface models can still provide a reasonable approximation for trajectory planning and comparative analysis, particularly when the primary objective is to optimize geometric alignment and cortical bone engagement rather than to predict absolute mechanical strength. In this work, the focus was placed on identifying anatomically feasible and mechanically favorable trajectories under subject-specific constraints, rather than on detailed screw–bone interaction modeling.

Future work may address this limitation by incorporating explicit thread geometry into the screw model or by coupling the proposed planning framework with finite element analysis (FEA) to better capture thread-induced stress distributions. Alternatively,

doi:10.6342/NTU202604598

effective material properties or correction factors derived from experimental data could be applied to approximate the mechanical contribution of threads without substantially increasing computational cost.

doi:10.6342/NTU202604598

Chapter 6 Conclusion and Future Work

6.1 Conclusion

This thesis presents an automated framework for cortical bone trajectory (CBT) planning that integrates particle swarm optimization (PSO) with Hounsfield Unit (HU)–based bone characterization to jointly consider geometric feasibility and bone quality. By formulating CBT planning as a subject-specific optimization problem, the proposed method provides a flexible alternative to conventional rule-based approaches that rely on fixed angular guidelines and anatomical heuristics.

A central component of the proposed framework is the use of a cortical-oriented mask derived from the relative HU distribution within each segmented vertebra. This mask is incorporated directly into the optimization objective to encourage screw trajectories that preferentially engage higher-density cortical regions while maintaining anatomical safety constraints. Cohort-level HU analysis across 784 subjects further supports the validity of this strategy, demonstrating consistent high-density cortical regions within the vertebral ROI despite the volumetric dominance of cancellous bone.

Experimental results on lumbar vertebrae from L1 to L5 demonstrate that the proposed framework is capable of generating anatomically plausible CBT trajectories across diverse vertebral morphologies. More favorable planning outcomes were generally observed at lower lumbar levels, where larger vertebral dimensions and wider pedicle corridors provide a more permissive anatomical environment. In contrast, upper lumbar levels present increased anatomical constraints, occasionally leading to minor distal tip breaches, reflecting the inherent trade-off between cortical engagement and strict intraosseous containment.

The results also indicate that optimized trajectories derived from the proposed

doi:10.6342/NTU202604598

framework do not always coincide with commonly cited CBT angular conventions. This observation suggests that data-driven, patient-specific optimization may complement traditional heuristic rules by adapting trajectory design to individual anatomical and mechanical conditions rather than strictly adhering to population-level guidelines.

In summary, this thesis demonstrates the feasibility of combining optimization-based planning with HU-informed bone characterization for CBT trajectory design. The proposed framework provides a foundation for future extensions toward more comprehensive patient-specific spinal screw planning and highlights the potential of computational optimization methods in supporting computer-assisted spine surgery.

6.2 Future Work

Future work will focus on further refining the angular calibration strategy to improve the consistency between mathematically optimized trajectories and clinically established CBT guidelines. By incorporating additional anatomical constraints and adaptive penalty terms, the framework is expected to achieve a better balance between computational optimality and clinical interpretability.

In addition, although the present study concentrates on lumbar vertebrae, the proposed methodology has the potential to be extended to the entire spine, including the cervical and thoracic regions, where anatomical complexity and safety requirements are even more critical. Adapting the framework to these regions will require the integration of region-specific anatomical models and safety constraints to ensure reliable trajectory planning across different spinal levels.

Another important direction for future development is the incorporation of finite element analysis (FEA) into the optimization pipeline. By coupling trajectory planning

doi:10.6342/NTU202604598

with biomechanical simulation, the current geometry- and HU-based evaluation can be augmented with mechanical performance indicators such as stress distribution, pullout strength, and stability under physiological loading. This integration would enable a more comprehensive and clinically relevant assessment of optimized trajectories and further strengthen the practical value of the proposed framework.

doi:10.6342/NTU202604598

REFERENCE

BOOKS

[1] A. Abd-Elsayed, Ed., Spinal Fusion Techniques, 1st ed. Philadelphia, PA, USA: Elsevier, 2024.

[2] A. P. Dhawan, Medical Image Analysis, 2nd ed. Oxford, U.K.: Wiley-Blackwell, 2011.

PERIODICALS

[3] GBD 2021 Low Back Pain Collaborators, "Global, regional, and national burden of low back pain, 1990–2020, its attributable risk factors, and projections to 2050: A systematic analysis of the Global Burden of Disease Study 2021," Lancet Rheumatology, vol. 5, no. 6, pp. e316–e329, May 2023, doi: 10.1016/S2665-9913(23)00098-X.

[4] M. R. Zindrick, "The role of transpedicular fixation systems for stabilization of the lumbar spine," Orthop. Clin. North Am., vol. 22, no. 2, pp. 333–344, 1991, doi: 10.1016/S0030-5898(20)31658-8.

[5] B. G. Santoni, R. A. Hynes, K. C. McGilvray, G. Rodriguez-Canessa, A. S. Lyons, M. A. Henson, W. J. Womack, and C. M. Puttlitz, "Cortical bone trajectory for lumbar pedicle screws," Spine J., vol. 9, no. 5, pp. 366–373, May 2009, doi: 10.1016/j.spinee.2008.07.008.

[6] J. Zheng, Y. Wu, C. Guo, X. Fang, and T. Ding, "Efficacy and safety of cortical bone trajectory screws versus pedicle screws in lumbar fusion: A systematic review and meta-analysis," World Neurosurg., vol. 188, pp. e233–e246, 2024, doi: 10.1016/j.wneu.2024.05.090.

doi:10.6342/NTU202604598

[7] S. Saleem, H. M. Aslam, M. A. Rehmani, A. Raees, A. A. Alvi, and J. Ashraf, "Lumbar disc degenerative disease: Disc degeneration symptoms and magnetic resonance image findings," Asian Spine J., vol. 7, no. 4, pp. 322–334, 2013, doi: 10.4184/asj.2013.7.4.322.

[8] A. N. Khan, H. E. Jacobsen, J. Khan, C. G. Filippi, M. Levine, R. A. Lehman Jr., K. D. Riew, L. G. Lenke, and N. O. Chahine, "Inflammatory biomarkers of low back pain and disc degeneration: A review," Ann. N. Y. Acad. Sci., vol. 1410, no. 1, pp. 68–84, 2017, doi: 10.1111/nyas.13551.

[9] S. Genevay and S. J. Atlas, "Lumbar spinal stenosis," Best Pract. Res. Clin. Rheumatol., vol. 24, no. 2, pp. 253–265, 2010.

[10] J. N. Katz and M. B. Harris, "Clinical practice: Lumbar spinal stenosis," N. Engl. J. Med., vol. 358, no. 8, pp. 818–825, 2008.

[11] L. Kalichman and D. J. Hunter, "Diagnosis and conservative management of degenerative lumbar spondylolisthesis," Eur. Spine J., vol. 17, no. 3, pp. 327–335, 2008.

[12] D. K. Sengupta and H. N. Herkowitz, "Degenerative spondylolisthesis: Review of current trends and controversies," Spine, vol. 30, no. 6, pp. S71–S81, 2005.

[13] M. Aebi, "The adult scoliosis," Eur. Spine J., vol. 14, no. 10, pp. 925–948, 2005.

[14] J. K. Birknes, A. P. White, T. J. Albert, C. I. Shaffrey, and J. S. Harrop, "Adult degenerative scoliosis: A review," Neurosurgery, vol. 63, no. 3, pp. A94–A103, 2008.

[15] NIH Consensus Development Panel on Osteoporosis Prevention, Diagnosis, and Therapy, "Osteoporosis prevention, diagnosis, and therapy," JAMA, vol. 285, no. 6, pp. 785–795, 2001.

[16] S. L. Silverman, "The clinical consequences of vertebral compression fracture,"

doi:10.6342/NTU202604598

Bone, vol. 13, pp. S27–S31, 1992.

[17] J. L. Old and M. Calvert, "Vertebral compression fractures in the elderly," Am. Fam. Physician, vol. 69, no. 1, pp. 111–116, 2004.

[18] T. Hirano, K. Hasegawa, H. E. Takahashi, et al., "Structural characteristics of the pedicle and its role in screw stability," Spine, vol. 22, no. 21, pp. 2504–2509, 1997.

[19] B. M. Frankel, S. D'Agostino, and C. Wang, "A biomechanical cadaveric analysis of polymethylmethacrylate-augmented pedicle screw fixation," J. Neurosurg. Spine, vol. 7, no. 1, pp. 47–53, 2007.

[20] M. Bydon, R. De la Garza-Ramos, M. Macki, A. Baker, A. K. Gokaslan, and A. Bydon, "Lumbar fusion versus nonoperative management for treatment of discogenic low back pain: A systematic review and meta-analysis of randomized controlled trials," J. Spinal Disord. Tech., vol. 27, no. 5, pp. 297–304, 2014.

[21] M. B. Kabins and J. N. Weinstein, "The history of vertebral screw and pedicle screw fixation," Iowa Orthop. J., vol. 11, pp. 127–136, 1991.

[22] V. Kosmopoulos and C. Schizas, "Pedicle screw placement accuracy: A meta-analysis," Spine, vol. 32, no. 3, pp. E111–E120, 2007.

[23] K. Matsukawa, Y. Yato, and H. Imabayashi, "Impact of screw diameter and length on pedicle screw fixation strength in osteoporotic vertebrae: A finite element analysis," Asian Spine J., vol. 15, no. 5, pp. 566–574, 2021, doi: 10.31616/asj.2020.0353.

[24] C. K. Lee et al., "An optimal cortical bone trajectory technique to prevent early surgical complications," Br. J. Neurosurg., pp. 1–7, 2020, doi: 10.1080/02688697.2020.1821172.

[25] C. C. Chang, H. K. Chang, C. C. Ko, et al., "Comparison of cortical bone trajectory to pedicle-based dynamic stabilization: An analysis of 291 patients," Neurospine,

doi:10.6342/NTU202604598

vol. 20, no. 1, pp. 308–316, 2023, doi: 10.14245/ns.2244888.444.

[26] K. Kojima, S. Asamoto, and Y. Kobayashi, "Cortical bone trajectory and traditional trajectory—a radiological evaluation of screw-bone contact," Acta Neurochir., vol. 157, pp. 1173–1178, 2015.

[27] K. Matsukawa, E. Taguchi, Y. Yato, H. Imabayashi, N. Hosogane, T. Asazuma, and K. Nemoto, "Evaluation of the fixation strength of pedicle screws using cortical bone trajectory," Spine, vol. 40, no. 15, pp. E873–E878, 2015.

[28] K. Matsukawa, Y. Yato, O. Nemoto, H. Imabayashi, T. Asazuma, and K. Nemoto, "Morphometric measurement of cortical bone trajectory for lumbar pedicle screw insertion using computed tomography," J. Spinal Disord. Tech., vol. 26, no. 6, pp. E248–E253, 2013.

[29] K. Matsukawa, Y. Yato, H. Imabayashi, N. Hosogane, T. Asazuma, and K. Nemoto, "Biomechanical evaluation of the fixation strength of lumbar pedicle screws using cortical bone trajectory: A finite element study," J. Neurosurg. Spine, vol. 23, no. 4, pp. 471–478, 2015.

[30] K. Matsukawa, "The cortical bone trajectory screws—indications and limits," in Modern Thoraco-Lumbar Implants for Spinal Fusion, Cham: Springer, 2018.

[31] K. T. Kim, M. G. Song, Y. J. Park, D. Y. Lee, and D. H. Kim, "Cortical trajectory screw fixation in lumbar spine surgery: A review of the existing literature," Asian Spine J., vol. 16, no. 1, pp. 127–140, 2022.

[32] W. K. Cheng, Y. T. Akpolat, S. İnceoğlu, S. Patel, and O. A. Danisa, "Pars and pedicle fracture and screw loosening associated with cortical bone trajectory," Spine J., vol. 16, no. 2, pp. e59–e65, 2016.

[33] F. Penner, N. Marengo, M. Ajello, S. Petrone, F. Cofano, F. Zenga, and D. Garbossa, "Preoperative 3D CT planning for cortical bone trajectory screws: A retrospective

doi:10.6342/NTU202604598

radiological cohort study," World Neurosurg., vol. 126, pp. e1468–e1474, 2019.

[34] K. Maruo, F. Arizumi, K. Kusuyama, K. Kishima, and T. Tachibana, "Accuracy and safety of cortical bone trajectory screw placement using patient-specific guides," J. Clin. Neurosci., vol. 78, pp. 147–152, 2020.

[35] R. Fujita, I. Oda, H. Tanaka, et al., "Real-world clinical accuracy of long cortical bone trajectory screw placement using a patient-specific template guide," J. Spine Surg., vol. 10, no. 3, pp. 468–478, 2024.

[36] Y. H. Zhang et al., "Anatomical study of the ideal cortical bone trajectory in the lumbar spine," Medicine, vol. 100, no. 2, p. e24099, 2021.

[37] J. Delgado-Fernández et al., "Simulation with 3D neuronavigation for learning cortical bone trajectory screw placement," J. Neurol. Surg. A, vol. 82, no. 3, pp. 262–269, 2021..

[38] Y. Deng et al., "CTSpine1K: A large-scale dataset for spinal vertebrae segmentation in computed tomography," arXiv preprint, arXiv:2105.14711, 2021.

[39] J. Kennedy and R. Eberhart, "Particle swarm optimization," in Proc. IEEE Int. Conf. Neural Networks, Perth, Australia, 1995, pp. 1942–1948.

[40] M. J. D. Powell, "An efficient method for finding the minimum of a function of several variables without calculating derivatives," Comput. J., vol. 7, no. 2, pp. 155–162, 1964.

doi:10.6342/NTU202604598

APPENDIX

- Hyperparameter Sensitivity Analysis Data:

This appendix provides the comprehensive numerical results for the Particle Swarm Optimization (PSO) hyperparameter tuning. These tables details the mean performance scores and computational runtimes for all tested combinations of swarm sizes ($N \in \{50, 60, 70, 80, 90, 100\}$) and iteration counts ($I \in \{100, 120, 140, 160, 180, 200\}$). All experiments were conducted on an NVIDIA A40 GPU to ensure runtime consistency. The evaluation metrics are presented across two tables: Table A 1 details anatomical segmentation performance, categorized by metric prefixes Cortical (Cortical Bone Score) and Vertebral (Vertebral Bone Score). Table A 2 reports the C/B_Ratio (Cortical-to-Trabecular Ratio) and Total_Time (Computational Runtime in seconds). For each metric, the following statistical indicators are reported across 10 independent trials:

- **_AVG**: Mean value.
- **_STD**: Standard Deviation.
- **_CV**: Coefficient of Variation ($CV = STD/AVG$), used to assess convergence stability.

doi:10.6342/NTU202604598

Table A 1. Performance metrics for anatomical segmentation across tested configurations (Swarm Size vs. Iterations): Cortical and Vertebral bone analysis.

Swarm_Size	Iteration	Cortical_AVG	Cortical_STD	Cortical_CV	Vertebral_AVG	Vertebral_STD	Vertebral_CV
50	100	82.26	5.9525	0.0724	94.01	2.0092	0.0214
50	120	83.45	4.1464	0.0497	93.57	2.6203	0.0280
50	140	82.82	5.2440	0.0633	93.28	2.5448	0.0273
50	160	82.98	3.5094	0.0423	94.32	2.7434	0.0291
50	180	80.80	4.5889	0.0568	90.97	3.3387	0.0367
50	200	82.80	3.0461	0.0368	92.81	2.3700	0.0255
60	100	84.18	4.0412	0.0480	94.03	2.3399	0.0249
60	120	82.89	3.5641	0.0430	92.97	3.0177	0.0325
60	140	82.35	5.0095	0.0608	93.47	3.5714	0.0382
60	160	84.70	1.6443	0.0194	93.65	2.2708	0.0242
60	180	81.29	7.1686	0.0882	93.07	5.3546	0.0575
60	200	84.04	3.4579	0.0411	94.10	3.2202	0.0342
70	100	84.82	3.6288	0.0428	94.35	2.1561	0.0229
70	120	82.56	6.4553	0.0782	93.93	3.2987	0.0351
70	140	81.73	2.9310	0.0359	92.80	1.5525	0.0167
70	160	83.37	5.7056	0.0684	94.71	2.9493	0.0311
70	180	80.31	7.9856	0.0994	91.23	5.6540	0.0620
70	200	81.90	3.9821	0.0486	92.57	2.8951	0.0313
80	100	83.26	4.9804	0.0598	93.43	3.3044	0.0354
80	120	83.12	5.3196	0.0640	92.62	3.9871	0.0430
80	140	83.67	5.5334	0.0661	93.62	3.9950	0.0427
80	160	83.31	5.2874	0.0635	93.42	4.7714	0.0511
80	180	84.50	2.2689	0.0269	95.24	1.1167	0.0117
80	200	83.41	2.7703	0.0332	93.51	2.1240	0.0227
90	100	82.82	3.7211	0.0449	93.11	3.3807	0.0363
90	120	83.25	5.5479	0.0666	93.70	3.2413	0.0346
90	140	83.79	3.2223	0.0385	93.64	2.8633	0.0306
90	160	83.82	2.7208	0.0325	94.22	1.3610	0.0144
90	180	82.29	3.1609	0.0384	92.86	2.3455	0.0253
90	200	82.88	5.7087	0.0689	94.44	2.7783	0.0294
100	100	83.93	4.1332	0.0492	94.58	3.3682	0.0356
100	120	82.83	3.2937	0.0398	92.87	2.2443	0.0242
100	140	85.22	3.9205	0.0460	94.68	3.1681	0.0335
100	160	84.04	5.5587	0.0661	95.13	3.0456	0.0320
100	180	84.38	4.8304	0.0572	94.27	3.6119	0.0383
100	200	83.05	1.9966	0.0240	94.05	2.5554	0.0272

doi:10.6342/NTU202604598

Table A 2. Cortical-to-trabecular ratio and computational runtime metrics across tested configurations (Swarm Size vs. Iterations).

Swarm_Size	Iteration	C/B_Ratio_AVG	C/B_Ratio_CV	C/B_Ratio_STD	Total_Time_AVG	Total_Time_STD	Total_Time_CV
50	100	0.8750	0.0515	0.0451	60.19	3.0028	0.0499
50	120	0.8917	0.0206	0.0183	72.48	1.2155	0.0168
50	140	0.8867	0.0354	0.0314	85.72	3.3299	0.0388
50	160	0.8800	0.0203	0.0179	99.37	1.4264	0.0144
50	180	0.8883	0.0337	0.0299	110.42	2.8220	0.0256
50	200	0.8917	0.0250	0.0223	122.50	1.1270	0.0092
60	100	0.8967	0.0251	0.0225	72.42	1.8209	0.0251
60	120	0.8933	0.0262	0.0234	89.59	1.7157	0.0192
60	140	0.8800	0.0313	0.0276	104.28	0.8729	0.0084
60	160	0.9025	0.0210	0.0189	116.15	1.1432	0.0098
60	180	0.8717	0.0426	0.0371	132.96	1.8652	0.0140
60	200	0.8950	0.0169	0.0152	146.86	2.5521	0.0174
70	100	0.8983	0.0227	0.0204	84.93	1.6020	0.0189
70	120	0.8783	0.0480	0.0422	104.67	1.8467	0.0176
70	140	0.8800	0.0269	0.0237	121.84	1.6482	0.0135
70	160	0.8800	0.0373	0.0329	138.17	2.8791	0.0208
70	180	0.8800	0.0407	0.0358	153.02	3.1767	0.0208
70	200	0.8850	0.0211	0.0187	170.85	3.5591	0.0208
80	100	0.8917	0.0278	0.0248	99.52	2.6005	0.0261
80	120	0.8967	0.0241	0.0216	116.82	2.9438	0.0252
80	140	0.8950	0.0306	0.0274	138.46	0.6147	0.0044
80	160	0.8950	0.0242	0.0217	157.12	0.9695	0.0062
80	180	0.8867	0.0233	0.0207	178.69	1.0047	0.0056
80	200	0.8917	0.0218	0.0194	194.87	1.7180	0.0088
90	100	0.8883	0.0132	0.0117	110.24	3.0041	0.0273
90	120	0.8867	0.0395	0.0350	130.72	3.5087	0.0268
90	140	0.8950	0.0117	0.0105	155.40	2.1233	0.0137
90	160	0.8900	0.0256	0.0228	177.53	0.8256	0.0047
90	180	0.8867	0.0210	0.0186	196.63	4.1689	0.0212
90	200	0.8767	0.0443	0.0388	223.32	6.7768	0.0303
100	100	0.8900	0.0142	0.0126	122.55	2.2229	0.0181
100	120	0.8917	0.0218	0.0194	147.04	1.7049	0.0116
100	140	0.9000	0.0141	0.0126	167.73	2.9830	0.0178
100	160	0.8817	0.0376	0.0331	196.56	3.9543	0.0201
100	180	0.8933	0.0220	0.0197	218.14	4.5982	0.0211
100	200	0.8817	0.0085	0.0075	245.94	0.7660	0.0031

doi:10.6342/NTU202604598